Final Quarterly Technical Report

MODELING OF TRANSIONOSPHERIC RADIO PROPAGATION

By: E. J. FREMOUW C. L. RINO

Prepared for:

ROME AIR DEVELOPMENT CENTER
GRIFFISS AIR FORCE BASE
ROME, NEW YORK 13441

Attention: MR. RICHARD A. SCHNEIBLE
(OCSE)

CONTRACT F30602-74-C-0279

Sponsored by

DEFENSE ADVANCED RESEARCH PROJECTS AGENCY
ARPA ORDER NO. 2777

SRI
STANFORD RESEARCH INSTITUTE
Menlo Park, California 94025 · U.S.A.

STANFORD RESEARCH INSTITUTE
Menlo Park, California 94025 · U.S.A.

(9) Final Quarterly Technical Report. 16 Feb - 14 May 75.
Covering the Period 16 February through 14 May 1975

(11) August 1975

(12) 54 p.

(6) MODELING OF TRANSIONOSPHERIC RADIO PROPAGATION

(10)
By: E. J. FREMOUW C. L. RINO

Prepared for:

ROME AIR DEVELOPMENT CENTER
GRIFFISS AIR FORCE BASE
ROME, NEW YORK 13441
Attention: MR. RICHARD A. SCHNEIBLE
(OCSE)
(315) 330-3085

(15) CONTRACT F30602-74-C-0279, ARPA Order - 2777
Effective Date of Contract: 15 May 1974
Contract Expiration Date: 14 May 1975
Amount of Contract: $99,542
Principal Investigator: E. Fremouw
(415) 326-6200, Ext. 2596
ARPA Order No. 2777
Program Code No. 44E20

Sponsored by:

DEFENSE ADVANCED RESEARCH PROJECTS AGENCY
1400 WILSON BOULEVARD
ARLINGTON, VIRGINIA 22209
Attention: MR. JAMES C. GOODWIN
STRATEGIC TECHNOLOGY OFFICE

SRI Project 3416

Copy No. 33

332 500

B

CONTENTS

ILLUSTRATIONS

TABLES

I REPORT SUMMARY

This is the final quarterly technical report on a one-year contract to extend and improve an existing empirical model for worldwide behavior of ionospherically imposed radio-wave scintillation. The objectives of the project were (1) to improve the accuracy of model-based calculations of the intensity-scintillation index and (2) to develop a capability for full description (from the point of view of engineering applications) of the first-order, complex-signal statistics that characterize the trans-ionospheric radio communication channel. A follow-on project has been initiated to extend the channel model to include second-order signal statistics in the temporal, spatial, and spectral domains. The first priority in the follow-on work will be to calculate the fluctuation spectra of relevant signal parameters. In addition, it is intended to extend validity of the model into the multiple-scatter regime.

The stated objectives of the just-completed project were accomplished by starting with the scintillation model developed by Fremouw and Rino (1973), adding a geomagnetic-activity dependence for the behavior of scintillation-producing ionospheric irregularities, and substituting a more accurate and general scattering theory for that of Briggs and Parkin (1963) used in the earlier model. The results of these efforts have been implemented in two computer programs. The first, entitled RFMOD, contains the main elements of the scattering theory, the morphological model for ionospheric irregularity strength and other parameters, and subroutines for calculating the geometry and other relevant quantities from user-specified inputs. The main outputs of RFMOD are the intensity-scintillation index S_4, which is the fractional rms fluctuation in received signal intensity (Briggs and Parkin, 1963), and an analogous phase scintillation index Φ_{rms} (labled PRMS), which is the rms fluctuation of phase.

Three related first-order, signal-statistical parameters also are output from RFMOD, to be used as inputs to the second program, called DIST. The latter program permits calculation of the first-order distribution functions of amplitude and phase for selected values of S_4 and/or Φ_{rms}. There are three types of output from DIST: values of the probability density functions (pdf) for amplitude and for phase, and values of the cumulative probability function (cpf) for intensity (or, equivalently, for amplitude since the argument is output in dB relative to the undisturbed level). The cpf output constitutes estimation of fade margin required to combat amplitude scintillation.

RFMOD and DIST represent interim versions of evolving transionospheric communication-channel codes. As stated above, capabilities will be added for calculating second-order statistics. More relevant in the near term is that there has been no direct testing of calculations relating to phase scintillation. As was recognized at the outset of the project, data are not available at present that are directly relevant to testing phase statistics unambiguously. Useful data are expected from forthcoming observations of multifrequency coherent satellite beacons, and such tests will be made. The forthcoming data may also result in model changes that will further alter the calculated results for amplitude scintillation, because testing to date has still necessarily relied on some observations reported in terms of a partly subjective scintillation index. In addition, while the assumption of weak, single scatter contained in the Briggs-and-Parkin theory has been partially removed, a more complete correction for multiple scatter effects has yet to be incorporated.

This report represents a summary of the work performed during the past year and is inteded as a status report on the evolving SRI/ARPA channel model. Section II describes the scattering theory employed and

compares some of its salient points with those of other theories. That section includes some material reported in earlier quarterly reports, for the sake of presenting a coherent discussion under one cover, but there is no attempt to describe the theoretical development in chronological detail. Section III contains a brief review of the known morphology of scintillation-producing ionospheric irregularities as modeled in RFMOD. A functional description of the programs RFMOD and DIST is presented in Section IV, along with instructions for their use. Finally, in Section V, we present our conclusions on the utility and limitations of the channel model in its present form and some prospects for further improvement.

II SCATTERING THEORY EMPLOYED

The basic approach to modeling the transionospheric communication channel is to treat the channel as a time-and-space-varying linear filter linking the transmitting and receiving antennas of a communication system. Slowly varying effects (on a time scale of many minutes or hours), such as group delay, polarization change, and dispersion of signals propagating through the smooth ionosphere, can be described by well-known deterministic methods and are not included in this work. What is treated are the relatively rapid and random variations (on a time scale of fractions of a second to a minute or so) in signal parameters that arise due to scattering by irregularities in ionospheric electron density and that are referred to as scintillations. Because the channel can be treated as a linear filter, standard Fourier techniques can be used to apply the results to modulated signals if a sufficiently general description is provided of the signal statistics resulting when a continuous (CW) is passed through the channel (Fremouw, 1969). In this section, we discuss the first-order statistics of this basic signal.

Any CW signal can be represented by a vector on the complex plane, such as the phasor E in Figure 1. In this figure, $E = \left(E_x + iE_y \right)$ is meant to represent the randomly time-varying complex amplitude of the signal output from an antenna terminal. In describing the first-order, complex-signal statistics of E, we are assessing the probability that the tip of the phasor lies within an elemental area on the complex plain. To begin, we write E as the resultant of its long-term mean $\langle E \rangle$ and a zero-mean, randomly varying component E_s. We choose to reference all phases to that of $\langle E \rangle$, which is the same as the phase that E would have in the

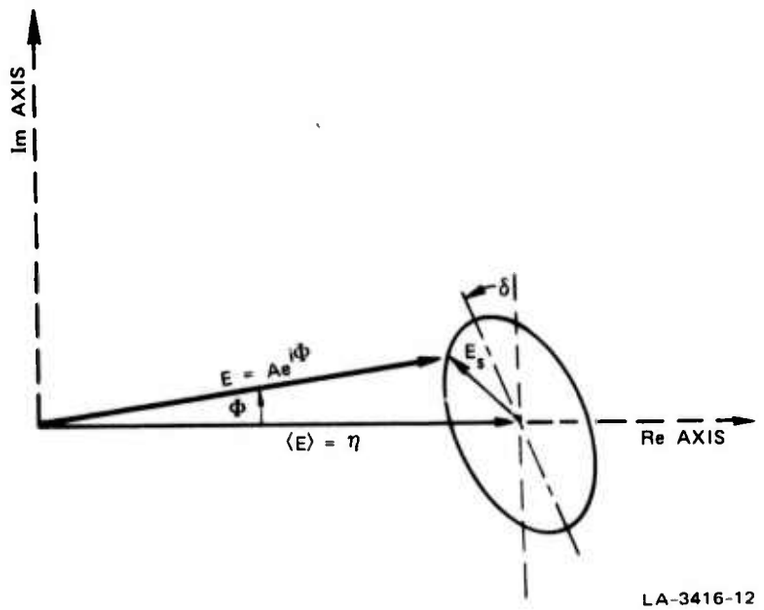

FIGURE 1 PHASOR DIAGRAM FOR CONSIDERATION OF FIRST-ORDER SIGNAL STATISTICS, SHOWING ELLIPTICAL CONTOUR OF EQUAL PROBABILITY PREDICTED BY THE GAUSSIAN-STATISTICS HYPOTHESIS

absence of channel-imposed perturbations because we have excluded slow channel variations from the model. (Thus $\langle E_y \rangle = 0$, and $\langle E_x \rangle \triangleq \eta = \langle E \rangle$.) The magnitude of $\langle E \rangle$ $(= \eta)$ is less than the amplitude of the undisturbed signal, however, because some of the transmitted energy has been scattered into the randomly varying component E_s.

To proceed with the analysis, it is convenient to break E_s into its own real and imaginary components, S_x and S_y, respectively. The convenience stems in part from the fact that the variances of S_x and S_y, σ_x^2 and σ_y^2, respectively, and their covariance σ_{xy}^2 can be calculated in terms of ionospheric parameters. These are useful calculations to perform because, at the very least, the sum of σ_x^2 and σ_y^2 represents the power contained in the scattered signal, which we shall denote as R_o. That is,

$$R_o = \langle E_s E_s^* \rangle = \sigma_x^2 + \sigma_y^2 \quad . \tag{1}$$

We shall normalize all our calculations to unity total received power, so R_o will represent the fraction of flux scattered--i.e., the forward-scattering coefficient of the ionosphere. A complex quantity analogous to the real R_o that it is useful is the following (Rino and Fremouw, 1973a):

$$B_o = \langle E_s E_s \rangle = (\sigma_x^2 - \sigma_y^2) + 2i\,\sigma_{xy}^2 \quad . \tag{2}$$

If it should be that the quadrature components, E_x and E_y, are jointly Gaussian random variables, the utility of the three variances defined above--or alternatively of R_o and B_o--would be very great. Indeed, in this instance the first-order statistics of the received signal E are totally defined by either of these sets of three parameters (i.e., the three real variances or the real R_o and the real and imaginary parts of B_o). Most scintillation observations have been only in terms of the magnitude of E (i.e., amplitude or intensity scintillation) because a sufficiently stable phase reference for measuring its complex value has seldom been available under scintillation conditions. Thus, there has been no direct determination of the complex-signal statistics. (This

data deficiency should be remedied within the next year by means of careful measurements of signals from the VHF-UHF coherent beacons on ATS-6 and the Transit satellites and, under a wider range of ionospheric conditions, by means of observations of the forthcoming DNA-002 multi-frequency beacon.)

The Gaussian-statistics hypothesis (i.e., that the quadrature components are jointly Gaussian variates) has been tested indirectly, however, by means of amplitude-scintillation data. Rino, Livingston, and Whitney (1975) assessed this hypothesis and the competing one of log-normal statistics (according to which the phase and the logarithm of amplitude are jointly Gaussian variates) by performing chi-square, goodness-of-fit tests of amplitude histograms to amplitude pdf's calculated from the two hypotheses. Good fits were found in general for both hypotheses, which tend toward identical pdf's as the scintillation index decreases, but the Gaussian hypothesis yielded better fits to 11 out of the 12 data sets tested. This result is fortunate because it permits presentation of scintillation calculations in a form that will be rather familiar to communications engineers. In the remainder of this report, we proceed on the basis of the Gaussian signal-statistics hypothesis.

For Gaussian signal statistics, a contour of equal probability for the tip of the E-phasor on the complex plane is an ellipse (Beckman and Spizzichino, 1963), such as the one in Figure 1. The analytical task of first-order, signal-statistical channel modeling, then, is to relate the parameters of such an ellipse to parameters of the channel (scattering irregularities in the ionosphere in the present case). The probability ellipse is characterized by its size, eccentricity, and orientation on the complex plane. Clearly, R_o (being the fraction of flux scattered) dictates the size of the ellipse. The eccentricity is dictated jointly by R_o and the magnitude of B_o, and the orientation is controlled by the phase angle of B_o. Specifically, the axial ratio of the probability ellipse is given by

$$r = \left[\frac{1 + \frac{|B_o|}{R_o}}{1 - \frac{|B_o|}{R_o}} \right]^{1/2} \tag{3}$$

and its orientation angle, δ (shown on Figure 1), is given by

$$\delta = \frac{1}{2} \angle B_o - \frac{\pi}{2} \tag{4}$$

It will be recognized from Eqs. (1) through (4) and the accompanying discussion that there are several sets of three parameters that can be used to describe the first-order, complex-signal statistics. For reasons of convenience, which will become clear in the ensuing discussion, we choose to work with the parameters R_o, $|B_o|/R_o$, and δ. As an example of the relationship of these three parameters to a quantity of direct applications interest, we have plotted the intensity-scintillation index S_4 in Figure 2 from the following formula derived by Nakagami (1960):

$$S_4^2 = 2R_o(1 - R_o)\left(1 - \frac{|B_o|}{R_o}\cos 2\delta\right) + R_o^2\left(1 + \frac{|B_o|^2}{R_o^2}\right) . \tag{5}$$

We note that in Briggs' and Parkin's theory, S_4 is calculated approximately as

$$S_4^2 \approx 2R_o\left(1 - \frac{|B_o|}{R_o}\cos 2\delta\right) . \tag{6}$$

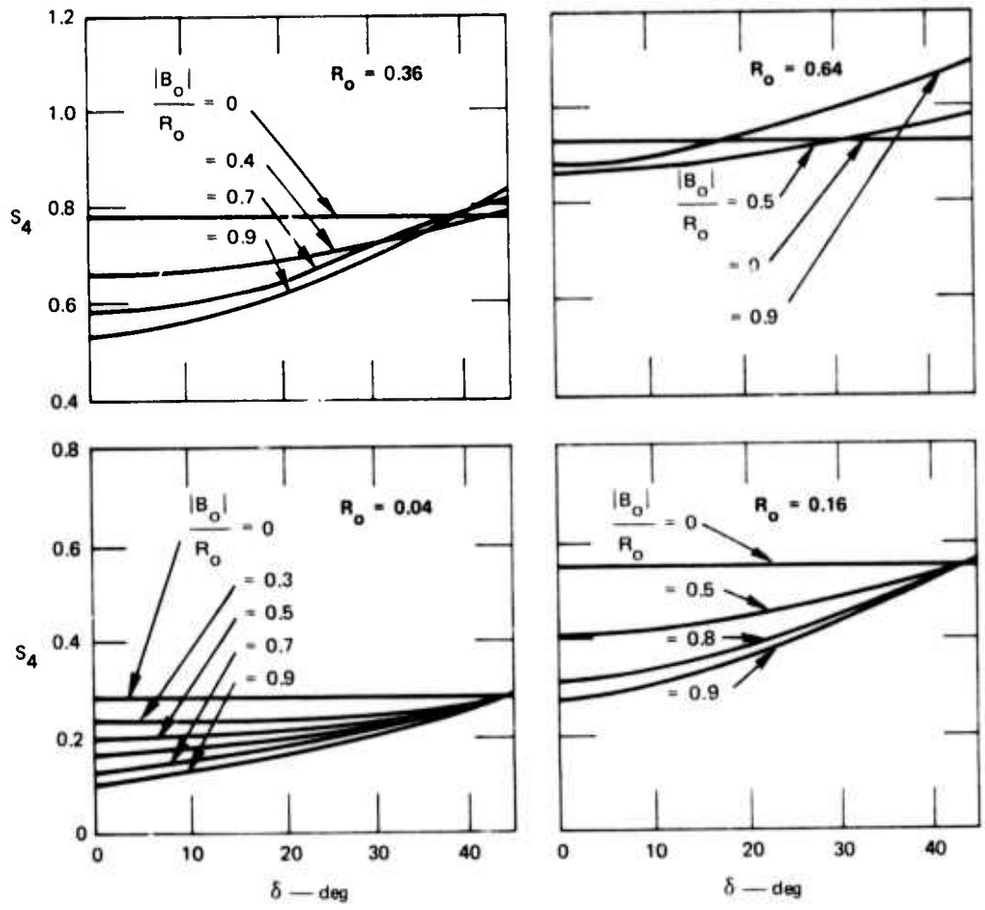

FIGURE 2 SCINTILLATION INDEX S_4 AS A FUNCTION OF ELONGATION AND ORIENTATION OF THE EQUAL-PROBABILITY ELLIPSE, FOR FOUR VALUES OF IONOSPHERIC SCATTERING COEFFICIENT, R_o

The following three relationships arise from Eqs. (1) and (2):

$$\sigma_x^2 = \frac{R_o}{2}\left[1 - \frac{|B_o|}{R_o}\cos(2\delta)\right] \tag{7}$$

$$\sigma_y^2 = \frac{R_o}{2}\left[1 + \frac{|B_o|}{R_o}\cos(2\delta)\right] \tag{8}$$

$$\sigma_{xy}^2 = \frac{-R_o}{2}\left[\frac{|B_o|}{R_o}\sin(2\delta)\right] . \qquad (9)$$

Thus, Eq. (6) contains only the contribution of the in-phase scattered component S_x to S_4. It arises from equating fluctuations in E_x to fluctuations in the real amplitude A and is accurate only for very weak scatter [i.e., when the higher-order R_o terms in Eq. (5) are negligible]. A significant improvement in the present scintillation model is retention of all terms in Eq. (5), which accounts for the contribution of fluctuations in the phase-quadrature component $E_y(=S_y)$ to amplitude scintillation (as well as for the influence of the correlation between S_x and S_y).

Other differences between the old scattering theory and the new arise in the manner of calculating R_o and B_o. The basic approach used in the present work is that described by Rino and Fremouw (1973b), in which the scattering geometry is treated quite rigorously. Briggs and Parkin simplified the geometry by assuming that the ionospheric scattering layer effectively can be tilted from the horizontal so that its boundaries are always normal to the incident radio-wave propagation vector. This approximation breaks down for large zenith angles but it avoids a great deal of complication in derivation of the scattering equations. Some of this complication was avoided by Rino and Fremouw (1973b) by assuming zero correlation in electron-density fluctuation along the vertical, which has negligible effect on the scattering equations for nearly vertical incidence. Again, however, the effect of the assumption becomes unacceptable as the incidence angle increases.

During the last quarter of this contract, the theory was recast to include the scattering effect of structure in all three dimensions of the ionosphere. An outline of the derivation is given here, together with the resulting equations for describing first-order signal statistics,

which are valid over a greater range of incidence angles than their counterparts in Quarterly Technical Reports 1 and 2.

The scattering coefficient R_o represents a special case of the spatial autocorrelation function of the scattered signal, which is defined as

$$R(\vec{\rho}) \triangleq \langle E_s(\vec{r})\, E_s^*(\vec{r} + \vec{\rho}) \rangle \; ; \tag{10}$$

namely, the case in which the spatial lag parameter $\vec{\rho}$ is zero. A similar definition, calculated without taking the complex conjugate, can be made of a quantity $B(\vec{\rho})$, which reduces B_o in the same special case (i.e., zero lag). The approach to evaluating $R(\vec{\rho})$ and $B(\vec{\rho})$ is to express E_s as the scattered field calculated by means of the first Born approximation, with the scattering medium represented by a spatial spectrum of ionospheric structure. The field is calculated by integrating the contribution from different heights within the scattering layer, considering the diffraction effects arising in propagation to the observing plane but ignoring effects of multiple scatter. When the complex field is multiplied by its complex conjugate, the effects cancel.

The result is that $R(\vec{\rho})$ can be expressed as the two-dimensional Fourier transform of a height-smeared version of the ionosphere's spatial spectrum and $B(\vec{\rho})$ can be expressed as the transform of that spectrum times a propagation factor. Setting the lag parameter to zero is tantamount to integrating over the spectra in the observing plane (as opposed to calculating the Fourier transforms), with R_o being an integral over the scattered field's angular power spectrum and B_o being an integral over a complex spectrum that incorporates diffraction effects.

Probably more important for first-order statistics than the approach to deriving R_o and B_o is the form of the spatial spectrum used in

their calculation. In evaluating R_o and the second factor in Eq. (6), Briggs and Parkin assumed a Gaussian-shaped spatial spectrum for the ionosphere. While convenient because of its Fourier-transformation characteristics, a Gaussian spectrum does not appear to represent ionospheric structure very realistically (Rufenach, 1972; Dyson et al., 1974).

A better description is afforded by a power law with a low-frequency cutoff. When normalized so that its three-dimensional integral is unity times the spatial variance $\langle(\Delta N)^2\rangle$ of electron density, such a spectrum [units of $(\text{electrons/m}^3)^2$ per unit three-dimensional spatial frequency, $\vec{\kappa}$] may be written as

$$\mathcal{H}(\vec{\kappa}) = 8\pi^{3/2} \frac{\Gamma(\nu + 1/2)}{\Gamma(\nu - 1)} \frac{\alpha^3 a \langle(\Delta N)^2\rangle}{\left\{1 + [\alpha S(\vec{\kappa})]^2\right\}^{\nu + 1/2}} \quad , \tag{11}$$

where ν is the spectral index defining the power law, α is scale-size parameter controlling the low-frequency cutoff, a is the ratio of irregularity scale size along the geomagnetic field to that across the field, and the three dimensional shape and orientation of the irregularities (Budden, 1965), are described by

$$S^2(\vec{\kappa}) = A(\psi)\, \kappa_x^2 + \kappa_y^2 + B(\psi)\kappa_z^2 - 2C(\psi)\kappa_x \kappa_z \quad , \tag{12}$$

where

$$A(\psi) = \frac{a^2 + C^2(\psi)}{B(\psi)} \quad , \tag{13}$$

$$B(\psi) = \cos^2 \psi + a^2 \sin^2 \psi \quad , \tag{14}$$

$$C(\psi) = (1 - a^2) \cos \psi \sin \psi \quad , \tag{15}$$

and ψ = the magnetic dip.

The coordinate system used is such that κ_x is directed to the geomagnetic north, κ_y to the geomagnetic east, and κ_z downward.

Using the above spectrum, one obtains the following expression for R_o:

$$R_o = 2\sqrt{\pi}\, r_e^2\, \lambda^2\, \frac{\Gamma(\nu - 1/2)}{\Gamma(\nu - 1)}\, \frac{a\, \alpha \sec^2 \theta}{\sqrt{A'C'}}\, L\langle(\Delta N)^2\rangle \quad , \tag{16}$$

where r_e = classical electron radius,

λ = observing wavelength,

L = thickness of scattering layer,

$A' = 1/2[D' + D]$,

$C' = 1/2[D' - D]$,

$D' = 1 + B(\psi + 90^\circ) + 2C(\psi) \tan \theta \cos \phi + B(\psi) \tan^2 \theta$,

$D = \sqrt{[D' - 2(1 + \sin^2 \phi)]^2 + (B')^2}$,

$B' = B(\psi) \tan^2 \theta \sin 2\phi + 2C(\psi) \tan \theta \sin \phi$,

θ = incidence angle on scattering layer,

and ϕ = propagation azimuth relative to geomagnetic north at height of scattering layer.

Eq. (16) was obtained by integrating analytically over the angular power spectrum of the scattered wave arriving at the observing plane, as described above. The integral over the complex spectrum associated with B_o cannot be performed analytically. However, the real and imaginary integrals involved have been solved numerically for a large range of

geometrical situations described by the parameters a, ψ, θ, and ϕ. Study of the numerical results has led to approximations suitable for implementation in an operating computer code such as RFMOD.

Simplifications have been found by converting the real and imaginary integrals to the magnitude and phase angle of B_o and then to the quantities $|B_o|/R_o$ and δ [the latter via Eq. (4)]. The simplification arises from an empirically noted approximate relationship between the latter two quantities, as described in detail in Quarterly Technical Reports 1 and 2. It permits approximate description of the complete first-order, complex-signal statistics from solution of the real integral alone. What is actually calculated is σ_x^2/R_o, which is related to $\mathrm{Re}\{B_o\}$ by Eq. (7).

Two approximations are involved in formulating this part of the problem. The first--neglect of a diffraction effect related to layer thickness--appears numerically to be valid essentially anywhere outside the scattering layer. The second holds so long as the spectrum of irregularities contributing to E_x fluctuations is cut off at the low-frequency end by diffraction effects rather than by an inherent cutoff of the ionospheric spatial spectrum. Both in-situ (Dyson et al., 1974) and scintillation observations (Rufenach, 1972; Rino, Livingston, and Whitney, 1975) support this view for all frequencies of interest. We have, therefore, proceeded on the basis of this "near-zone" approximation, but we have incorporated a test in RFMOD to safeguard against violation of the assumption underlying it. On the basis of these two approximations, one may write σ_x^2/R_o as follows:

$$\frac{\sigma_x^2}{R_o} = 2(\nu - 1/2)\ \frac{\sqrt{A'}}{(C')^{\nu}}\left(\frac{\lambda Z \sec\theta}{4\pi\alpha^2}\right)^{\nu - 1/2}$$

$$\int_0^{\infty} q^{-2\nu} \int_0^{2\pi} \frac{\sin^2 [q^2 \mathcal{T}(\theta,\phi')]}{[(\beta')^2 \cos^2 \varphi + \sin^2 \varphi]^{\nu + 1/2}} \, d\varphi \, dq \qquad (17)$$

where $\sqrt{\lambda Z}$ = Fresnel-zone radius at scattering layer

$$\mathcal{T}(\theta,\phi') = [1 + \tan \theta \cos^2 (\phi' - \varphi)]^2 \quad , \qquad (18)$$

and

$$\beta' = \sqrt{A'/C'}$$

$$\phi' = \phi - \frac{1}{2} \tan^{-1} \left[\frac{B'}{D' - 2(1 + \sin^2 \phi)} \right] \quad . \qquad (19)$$

The main diffraction effect dictating the first-order statistics of a scattered signal is controlled by the Fresnel-distance parameter appearing in parentheses in front of the integral in Eq. (17). The integral itself contains only geometric factors. Although the integral cannot be solved analytically, it has been possible to find a useful algebraic approximation to it. The approach was to numerically evaluate the integral, which was named $F(\beta', \theta, \phi,)$, for selected points in a three-space of β', θ, and ϕ', and then to fit judiciously chosen algebraic functions to the points. The resulting functions then were incorporated into RFMOD. The procedure was as follows.

First, the integral was solved numerically for $\beta' = 1$, 2, 5, 10, and 20, with θ ranging from 0° through 80° (which exceeds the maximum incidence angle of a transionospheric communication link on the F layer, by virture of the ionosphere's curvature), and with ϕ' stepped between 0° and 90° (since the ϕ' dependence is symmetrical about 90°). After the results were plotted, inspection of the curves suggested a behavior of the following form:

$$F(\beta', \theta, \phi') = \frac{1}{2} a(\beta', \theta) + b(\beta', \theta) + (b - a) \cos 2\phi', \qquad (20)$$

where a = the value of the integral when $\phi' = \pi/2$, and b = the value when $\phi' = 0$.

The values of a and b were then plotted as functions of θ for given values of β'. Again the plots suggested analytic fits of the form

$$a(\beta', \theta) = c(\beta') \sec \theta^{m(\beta')} \tag{21}$$

$$b(\beta', \theta) = c(\beta') \sec \theta^{n(\beta')} \tag{22}$$

where $c(\beta')$ = the value of the function when $\theta = \phi' = 0$ and where the exponents $m(\beta')$ and $n(\beta')$ were chosen by forcing Eqs. (21) and (22) to match the numerical value of the integral when $\theta = 70^\circ$, which is about its largest value for penetration of the F layer. The values of c, m, and n were then employed in a one-dimensional, least-squares fitting routine to obtain best-fit polynomial expansions of $c(\beta')$, $m(\beta')$, and $n(\beta')$.

The results of the above procedure were combined into an algebraic approximation to the integral in Eq. (17), and the approximation was then used to calculate curves of $F(\beta', \theta, \phi')$ over the ranges of θ and ϕ' and for the values of β' originally employed in the numerical integration. Finally, similar curves were calculated for other (both intermediate and more extreme) values of β', and numerical integrations were performed for these new cases. The entire collections of numerical-integration and algebraic-approximation results were then compared to determine the efficacy of the approximate expression. An example of the comparison is presented in Figure 3 for a value of β' not involved in development of the approximation; the smooth curves represent the algebraic fit and the individual points are results of the numerical integration. The fit is considered quite adequate for application to scintillation modeling. Thus, RFMOD contains the following expression:

$$\frac{\sigma_x^2}{R_o} = 2(\nu - \frac{1}{2}) \frac{\sqrt{A'}}{(C')^{\nu}} \left(\frac{\lambda Z \sec \theta}{4\pi\alpha^2} \right)^{\nu - \frac{1}{2}} F(\beta', \theta, \phi') \quad , \tag{23}$$

where $F(\beta', \theta, \phi')$ is calculated from Eq. (20).

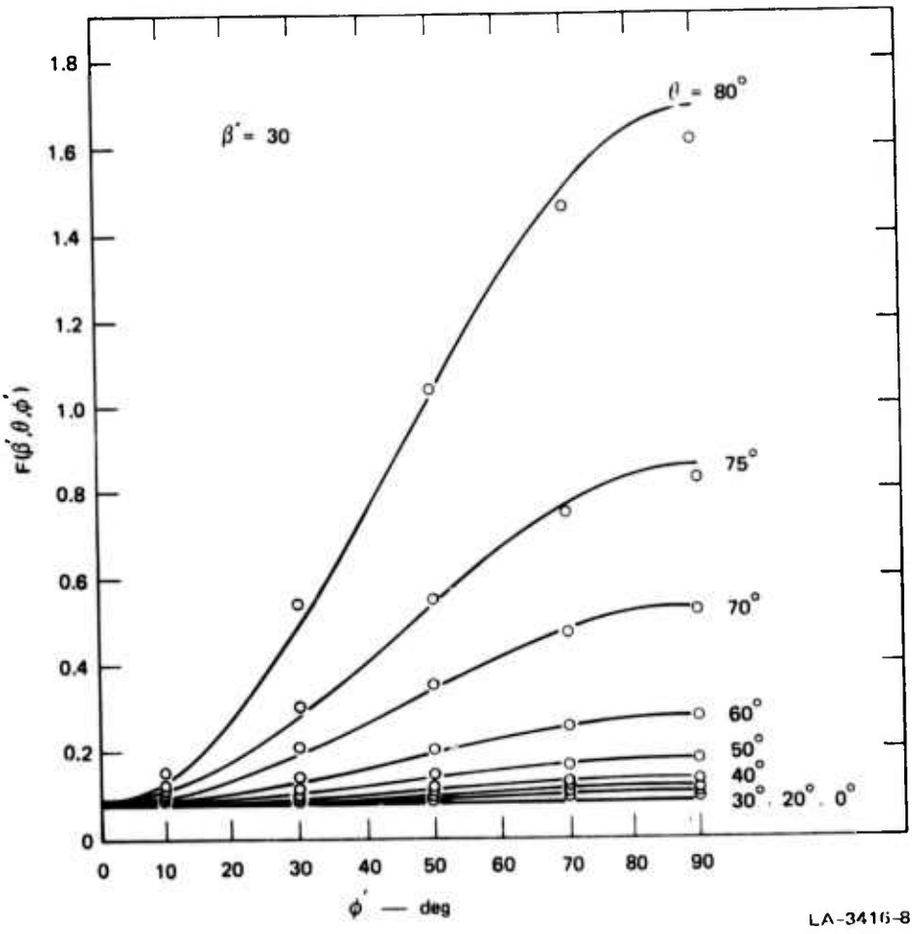

FIGURE 3 COMPARISON OF ALGEBRAIC APPROXIMATION (Eq. 20) TO VALUES OF THE INTEGRAL IN EQ (17)

It is clear from Eqs. (7), (8), and (9), that the first-order statistical problem would be completely solved at this point if one could find an approximation to σ_{xy}^2 in some manner analogous to that above for σ_x^2 (σ_y^2 being simply $R_o - \sigma_x^2$). However, no such approximate

solution to the imaginary part of the B_o integral has been found, and numerical integration each time RFMOD is run seems unacceptably inefficient. Fortunately, as mentioned above, synthesis of the numerical integration results that have been obtained has pointed to another simple procedure. Specifically, when $|B_o|/R_o$ and δ were formed from the real and imaginary integrals for a number of geometrical situations, it was found that the relationship between $|B_o|/R_o$ and δ was not very dependent on geometry and was well approximated by the following simple formula:

$$\delta = \frac{\pi}{4}\left(1 - |B_o|/R_o\right). \tag{24}$$

Not only is the relationship between δ and $|B_o|/R_o$ rather insensitive to geometry, but also the first-order signal statistics are not very sensitive to that relationship. For first-order statistics, the main effect of diffraction is a simultaneous rotation (increasing δ) and circularization (decreasing $|B_o|/R_o$) of the correlation ellipse illustrated in Figure 1, as the scattered wave propagates with increasing Z in Eq. (23). What is important is the rate at which this approach to Rice statistics ($|B_o|/R_o = 0$ and $\delta = 45^\circ$) takes place rather than the precise relation between ellipse elongation and eccentricity. Thus, we have proceeded on the basis of Eq. (24), which, when combined with Eq. (7), yields the following transcendental equation relating $|B_o|/R_o$ to σ_x^2/R_o:

$$\frac{|B_o|}{R_o}\left[\cos\frac{\pi}{2}\left(1 - \frac{|B_o|}{R_o}\right)\right] = 1 - 2\,\frac{\sigma_x^2}{R_o} \quad . \tag{25}$$

Eq. (25) is fit very well, especially in the near and intermediate zones, by the following approximation:

$$\frac{|B_o|}{R_o} = 0.98\left(1 - 1.55\,\frac{\sigma_x^2}{R_o}\right) \quad . \tag{26}$$

Inserting Eqs. (7) and (26) into Eq. (5), we obtain the following very useful formula for scintillation index:

$$S_4 = \left\{ 4R_o\left(\frac{\sigma_x^2}{R_o}\right) - 4R_o^2\left(\frac{\sigma_x^2}{R_o}\right) + R_o^2\left[1.98 - 1.52\left(\frac{\sigma_x^2}{R_o}\right)\right]\right\}^{1/2} . \qquad (27)$$

While containing some approximations in its third term, Eq. (27) is a considerable improvement over the formula of Briggs and Parkin for S_4 [Eq. (6)], which totally neglected both the second and third terms. The improvement increases as the scattering becomes more intense (increasing R_o).

One reason for separating the first two terms in Eq. (27) into two factors is that R_o is amenable to a simple multiple-scatter correction. The theory discussed so far is limited to the regime of weak, single scatter for the entire scattering region (i.e., $R_o \ll 1$). However, an important effect of multiple scatter, namely extinction of the non-scattered signal component (represented by $\langle E \rangle$ in Figure 1), can be accounted for simply by requiring conservation of total power flux while applying the first Born approximation to elemental layers within the scattering region. From the work of Fejer (1953), Bramley (1955), Fremouw (1968), and Rino (1975), it follows that extinction can be accounted for by replacing the single-scattering coefficient calculated from Eq. (16) by a multiple-scattering coefficient defined by

$$R_o' = 1 - e^{-R_o} . \qquad (28)$$

It is R_o' that is used (in place of R_o) in Eq. (27) for calculation of scintillation index, which is output as S4, in RFMOD; this multiple-scattering coefficient (R_o') is itself output from RFMOD as RZRO. An

important task for the second contract year is to find an analogous multiple-scatter correction for σ_x^2/R_o and the related quantities $|B_o|/R_o$ and δ. Presently, the latter two parameters are calculated from Eqs. (26) and (24), respectively, on the basis of Eq. (23). They are output from RFMOD as BMAGR and DELTA, respectively, for use as inputs to the second channel-model code, DIST. A single-scatter approximation warning is printed if $R_o \geq 1$.

Once R_o', $|B_o|/R_o$, and δ are calculated, then application of the Gaussian-statistics hypothesis permits calculation of any desired first-order, signal-statistical parameter. The calculation of the intensity-scintillation index,

$$S_4 \triangleq \frac{\langle (A^2 - \langle A^2 \rangle)^2 \rangle^{1/2}}{\langle A^2 \rangle} \tag{29}$$

as described above, is an example. An analogous phase-scintillation index may be defined as

$$\Phi_{rms} \triangleq \langle (\Phi - \langle \Phi \rangle)^2 \rangle^{1/2} \tag{30}$$

$$= (\langle \Phi^2 \rangle - \langle \Phi \rangle^2)^{1/2} \quad . \tag{31}$$

Given the phase reference chosen in Figure 1, it is well known (e.g., Beckman and Spizzichino, 1963) that under the postulate of Gaussian statistics, the joint probability density function (pdf) for the real, E_x, and imaginary, E_y, parts of the received signal's complex amplitude, E, is given by

$$p_{xy}(E_x,E_y) = \frac{1}{2\pi\sigma_x^2\sigma_y^2\sqrt{1-\rho^2}} \exp\left\{\frac{1}{2(1-\rho^2)}\left[\left(\frac{E_x - \eta}{\sigma_x}\right)^2 - 2\rho\,\frac{(E_x - \eta)E_y}{\sigma_x\sigma_y} + \frac{E_y^2}{\sigma_y^2}\right]\right\} \tag{32}$$

where $\rho = \sigma_{xy}^2/\sigma_x\sigma_y$ and where η may be calculated from $\eta = \sqrt{1 - R_o'}$ and the σ's from Eqs. (7), (8), and (9). The individual pdf's for amplitude and for phase can be calculated by changing variables in Eq. (32) from component to polar form and then integrating over the other variable. That is,

$$p(A) = \int_0^{2\pi} A\, p_{xy}(A\cos\Phi,\ A\sin\Phi)\, d\Phi \tag{33}$$

and

$$p(\Phi) = \int_0^{\infty} A\, p_{xy}(A\cos\Phi,\ A\sin\Phi)\, dA \quad . \tag{34}$$

Analytic solutions to the integrals in Eqs. (33) and (34) have been known for some time in special cases (e.g., for Rice statistics, in which $\sigma_{xy} = 0$ and $\sigma_x = \sigma_y$), but not so for the generalized Gaussian statistics needed to describe scintillation. Recently, however, Hatfield (1975) has found the following general analytic solution for Eq. (34):

$$p(\Phi) = \frac{\exp\left[\dfrac{-\dfrac{\eta^2}{\sigma_x^2} + f_2^2(\Phi)}{2(1-\rho^2)}\right]}{2\pi\sigma_x\sigma_y\sqrt{1-\rho^2}\, f_1^2(\Phi)} \left\{(1-\rho^2)\exp\left[\frac{-f_2^2(\Phi)}{2(1-\rho^2)}\right] + f_2(\Phi)\frac{\sqrt{2\pi(1-\rho^2)}}{2}\,\mathrm{erfc}\left[\frac{-f_2(\Phi)}{\sqrt{2(1-\rho^2)}}\right]\right\} \tag{35}$$

where $$f_1(\Phi) = \sqrt{\cos^2\Phi/\sigma_x^2 - 2\rho\cos\Phi\sin\Phi/(\sigma_x\sigma_y) + \sin^2\Phi/\sigma_y^2} \tag{36}$$

and $$f_2(\Phi) = \eta_x[\cos\Phi/\sigma_x^2 - \rho\sin\Phi/(\sigma_x\sigma_y)]/f_1(\Phi) \quad . \tag{37}$$

Unfortunately, there is no known analytic solution for the moments of the distribution in Eq. (35). Therefore, the distribution itself has been incorporated in RFMOD, together with a numerical integration routine for calculating its first and second moments, as follows:

$$\langle \Phi \rangle = \int_0^{2\pi} \Phi \, \rho \, (\Phi) \, d\Phi \tag{38}$$

and

$$\langle \Phi^2 \rangle = \int_0^{2\pi} \Phi^2 \, \rho \, (\Phi) \, d\Phi \quad . \tag{39}$$

The results of Eqs. (38) and (39) are then inserted into Eq. (31) for calculation of the phase-scintillation index, which is output as PRMS.

As described above, the signal-statistical outputs of RFMOD are R_o', $|B_o|/R_o$, δ, S_4, and Φ_{rms}. The last two outputs constitute an intensity-scintillation index and a phase-scintillation index, respectively, and represent our judgment as to the first-order statistical parameters most likely to be sought by a user for synoptic purposes. The other three outputs are provided for use in posing more detailed questions about first-order signal statistics in particular cases, by means of the DIST code.

The DIST code is essentially a device for calculating and outputing the amplitude and phase pdf's from inputs of R_o', $|B_o|/R_o$, and δ. For phase, it is simply a matter of evaluating Eq. (35) for the given input parameters and outputing the result as P(PHI). Unfortunately, there is no known analytical solution to Eq. (33) analogous to Hatfield's phase distribution. Thus, it is necessary to perform the phase integration over the joint distribution (32) numerically. This integration is performed in DIST, and the result is output as P(A) versus A (the latter in

units of undisturbed amplitude). In addition, the following integration also is performed numerically:

$$P(A < V) = \int_0^V \rho(A)\, dA \quad . \tag{40}$$

This resulting cumulative probability function (cpf) of amplitude is then output as CPF versus 20 log V (labeled dB). Since the independent variable is output in decibels, CPF may be thought of as the cumulative distribution of intensity ($I = A^2$) as well as of amplitude (A); it represents the link margin needed to mitigate scintillation fading to a desired reliability threshold.

III SCINTILLATION MORPHOLOGY MODELED

The major work performed on this contract was development and implementation of the generalized scattering theory described in Section II. The other important aspect of modeling the transionospheric scintillation channel is description of the ionosphere's scattering structure as a function of several variables. The structural characteristics that must be described pertain to the strength, size, and shape of the radio-wave-scattering irregularities and the thickness of the scattering layer. All the relevant parameters appear in Eq. (16). The shape of the irregularities is described by the ionospheric spatial spectrum [Eqs. (11) and (12)], which is characterized mainly by the power-law spectral index, ν, and by the ratio, a, of scale-size parameter along the geomagnetic field to that across it. The size of the irregularities is scaled by the cross-field scale-size parameter, α. The strength of the irregularities is described by the spatial variance of electron density $\langle(\Delta N)^2\rangle$, and the thickness of the scattering region is L.

In-situ measurements of the ionospheric spatial spectrum (Dyson et al., 1974) show a remarkably consistent spectral index, corresponding very nearly to the Kolmorov value of 4/3 for ν, under most ionospheric conditions; we have adopted this value as a constant in the model. The irregularity axial ratio, a, also has been taken as constant, with a value of 10, as a result of the data review performed by Fremouw and Rino (1973). There is no direct measurement of the outer scale, α; it is simply known to be large compared with a km or so (Rufenach, 1972; Dyson et al., 1974; Sagalyn et al., 1974). We have found that α = 3 km produces a good fit to the amplitude-scintillation data analyzed by Rino, Livingston, and Whitney (1975), and this value is currently employed as a constant in the model.

The remaining two ionospheric parameters, $\langle(\Delta N)^2\rangle$ and L, appear in the scintillation calculations only as a product. We have set L = 100 km as a representative value and have expressed the behavior of scintillation in terms of the following empirical model for the rms electron-density variation, $\langle(\Delta N)^2\rangle^{1/2}$:

$$\langle(\Delta N)^2\rangle^{1/2} = \Delta N_e(\lambda, T, D, R) + \Delta N_m(\lambda, T) + \Delta N_h(\lambda, T, K_p)$$

$$+ \Delta N_a(\lambda, T, K_p) \text{ el/m}^3 \tag{41}$$

where λ = geomagnetic latitude in degrees

T = time of day in hours,

D = day of the year out of 365,

R = sunspot number,

K_p = planetary magnetic index.

The terms in Eq. (41) are

$$\Delta N_e = (1.2 \times 10^9)(1 + 0.05R)\left[1 - 0.25 \cos \pi\left(\frac{D + 10}{91.25}\right)\right]\left\{\exp\left[-\left(\frac{T + 1.5}{6}\right)^2\right]\right.$$

$$\left. + \exp\left[-\left(\frac{T - 22.5}{T_D}\right)^2\right]\right\}\left\{\exp\left[-\left(\frac{\lambda}{12}\right)^2\right]\right\} \qquad T_D = \begin{cases} 3 \text{ if } T \le 22.5 \\ 6 \text{ if } T > 22.5 \end{cases} \tag{42}$$

$$\Delta N_m = (4.4 \times 10^8)\left(1 + 0.33 \cos \frac{\pi T}{12}\right)\left\{\exp\left[-\left(\frac{\lambda - 32.5}{15}\right)^2\right]\right\} \tag{43}$$

$$\Delta N_h = (2.0 \times 10^9)$$

$$\left\{1 + \text{erf}\left[\frac{\lambda - 68.5 + 1.82 K_p + (5 + 0.55 K_p) \cos(\pi T/12)}{18.7 - 0.36 K_p - (1 + 0.11 K_p) \cos(\pi T/12)}\right]\right\} \tag{44}$$

$$\text{and} \quad \Delta N_a = (1.1 \times 10^8) \left\{ K_p \exp\left[-\left(\frac{\lambda - 77 + 1.82\, K_p + 4 \cos(\pi T/12)}{0.32\, K_p} \right)^2 \right] \right\} \quad (45)$$

Eqs. (42) and (43) describe, respectively, the equatorial and mid-latitude behavior of scintillation, and the high-latitude behavior is described by Eqs. (44) and (45). All four terms of Eq. (41) contain the well-established nighttime maximum of scintillation. The equatorial term also includes a seasonal variation, displaying equinoctial maxima. The most complicated behavior occurs at high latitudes, above the "scintillation boundary" (Aarons et al., 1969). Equation (44) essentially describes the behavior of the boundary location as a function of time of day and geomagnetic activity, and Eq. (45) accounts for scintillation that is directly related to auroral activity.

In the Fremouw-and-Rino 1973 model, the relationship of scintillation to geomagnetic activity was not included. The only solar-terrestrial observable employed in the earlier model was the sunspot number, which was intended as a measure of epoch during a solar cycle. However, it is clear that the scintillation boundary migrates equatorward, along with the auroral oval, with increasing planetary magnetic activity (Aarons et al., 1963; Evans, 1974). This was known at the time the 1973 model was developed, but the dependence was excluded to avoid double accounting for other aspects of scintillation behavior, such as seasonal and solar-cycle variation.

Pope (1974) modified our high-latitude term to include a K_p dependence without checking on the possibility of seasonal double accounting. We have had five years of K_p values plotted and have found no troublesome seasonal dependence. We have, therefore, adopted Pope's basic revision of replacing the sunspot-number dependence in our old high-latitude term with a K_p dependence. We have not used his exact formulation, however, which deleted our earlier description of the variation in statistical

width of the scintillation boundary with its location. We find that there is such a variable-width behavior in the in-situ data of Sagalyn et al. (1974); it is described by the denominator of the error-function argument in Eq. (44).

Having incorporated a K_p dependence in Eq. (44), it was a simple extension to include the K_p-dependent migration of the auroral oval in Eq. (45). A more accurate index to use might be the auroral-electrojet index, AE, but we have elected to use only K_p for simplicity. The two magnetic indices, K_p and AE, are rather highly correlated, as shown in Figure 4. To avoid the necessity for a user to specify two magnetic indices rather than just one, we have elected to exclude AE from the model unless later analysis of scintillation data shows that including it would improve the model's accuracy significantly. In a similar vein, we have avoided including a geomagnetic dependence in the equatorial term, retaining instead the original sunspot-number dependence. Further experimental work is necessary before a reliable geomagnetic dependence can be incorporated in the equatorial term; a likely candidate for a magnetic index is D_{st}, the seasonal and solar-cycle behaviors of which are similar to those of scintillation.

In addition to the above modifications to the 1973 model, some of the constants employed have been changed. These changes stem partly from improved calibration of some data sets used in development of the original model. The data sets in question (Aarons et al., 1963; Koster, 1968; Joint Satellite Studies Group, 1968) were presented in terms of a hand-scaled scintillation index, SI (Whitney and Malik, 1968), which only recently (Whitney, 1974) has been calibrated reasonably accurately to S_4. It is still to be noted that the relation between SI and S_4 must be scintillation-rate dependent, and data characterized directly by S_4 are strongly preferred for modeling.

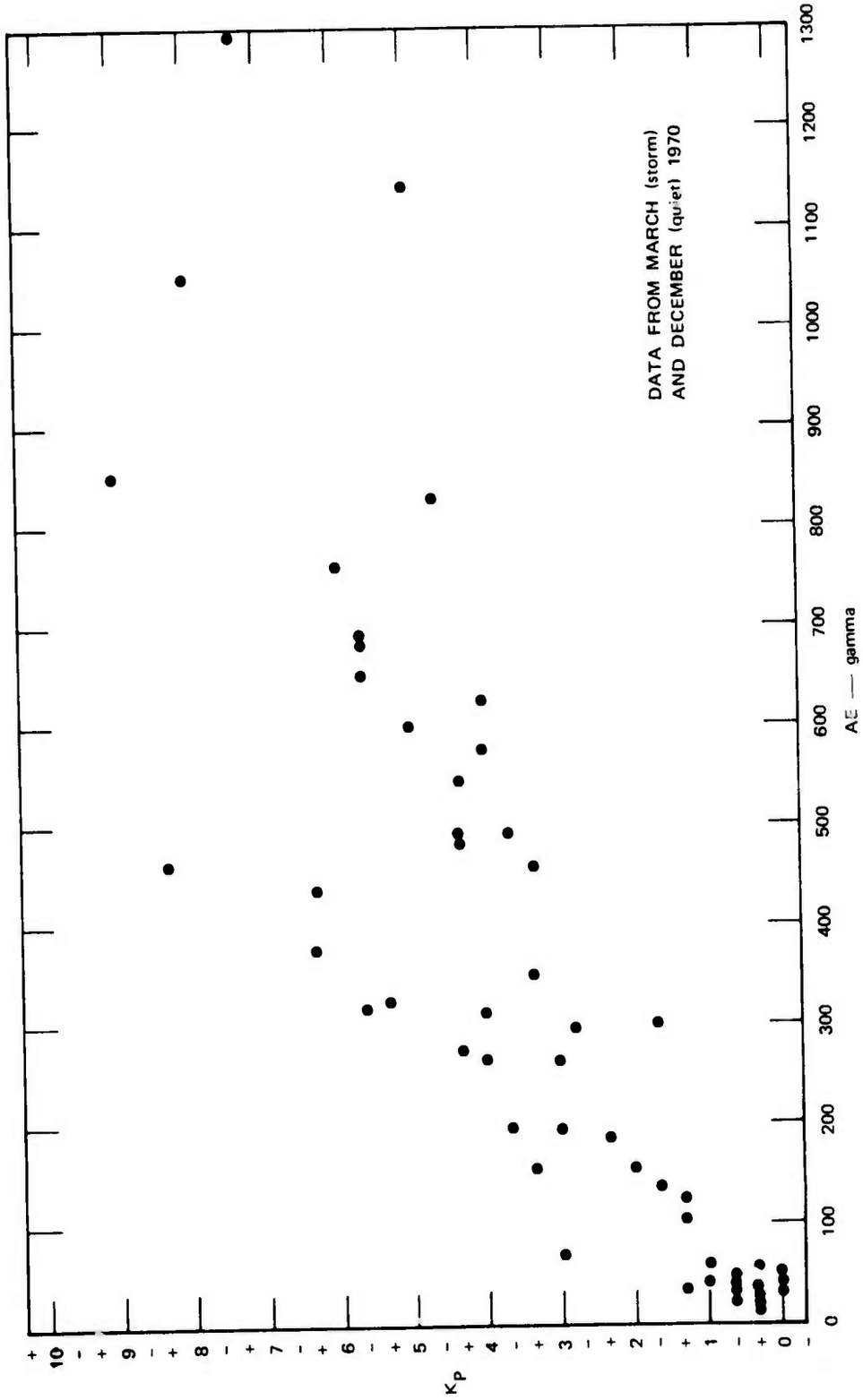

FIGURE 4 SCATTER PLOT SHOWING DEGREE OF CORRELATION BETWEEN AURORAL ELECTROJECT INDEX, AE, AND PLANETARY MAGNETIC INDEX, K_p

Figures 5 through 8 show the degree of fit between the model now in RFMOD and several data sets that were presented by the observers either in terms of S_4 or in terms of an empirical index such as SI, which we then converted to S_4. Figures 9 and 10 compare the amplitude pdf and cdf calculated by means of DIST with corresponding histograms developed from ATS 5 data provided by Aarons (private communication, 1974). The corresponding pdf for phase is shown in Figure 11; no phase data exist at this time for comparison.

IV THE CHANNEL-MODEL CODES

Of the two computer programs, RFMOD and DIST, the former is by far the more complicated. It is a modification of the program BPMOD, described by de la Beaujardiere and McNiel (1971), and consists of the routines listed in Table 1. Its very simplified flow chart is shown in Figure 12. Using RFMOD consists essentially of preparing input cards, of which there are three types: (1) a title card, (2) namelist cards, and (3) a changing-parameter(s) card. Three sample sets of input cards are shown in Figure 13, and each type of card is described below.

The title card is used to assign any desired title of up to 80 characters to a calculation case or series of cases. It is read by the driver program, RFMOD, into the array LBL with a 20A4 format, and printed in the output by the subroutine IMPRIME; it has no effect whatsoever on the rest of the program. Any number of cases can be run under a common title, which will be printed in the output for each case.

The namelist cards are used to input the fixed parameters for a calculation case. They are read by subroutine READIN, by means of the namelist INPAR. The user gives the name and desired value for each quantity listed above the dashed line in Table 2 that is to be fixed. The number under the heading K in Table 2 is an index used in the

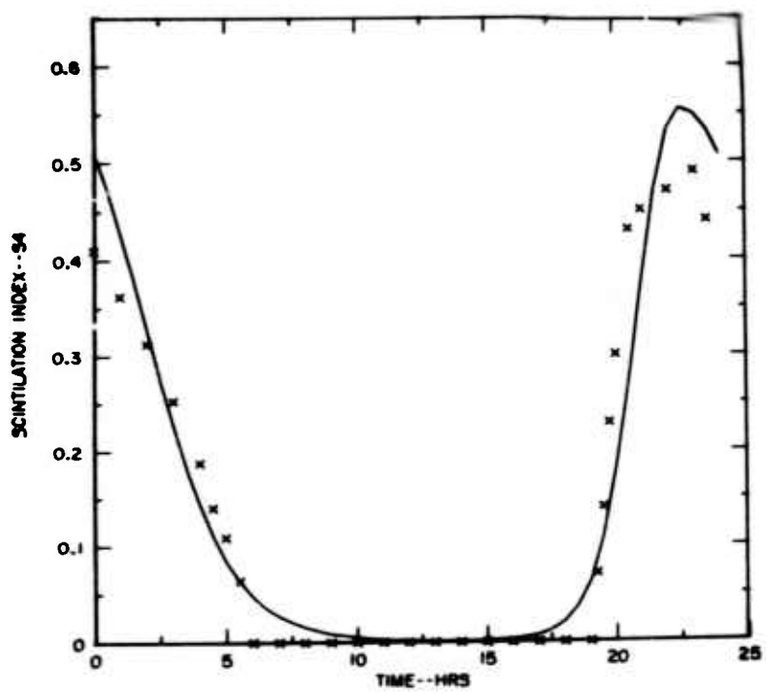

FIGURE 5 COMPARISON OF MODEL CALCULATION (solid curve) WITH DIURNAL VARIATION OF 136-MHz INTENSITY-SCINTILLATION INDEX OBSERVED (Xs) BY KOSTER (1968) IN THE EQUATORIAL REGION

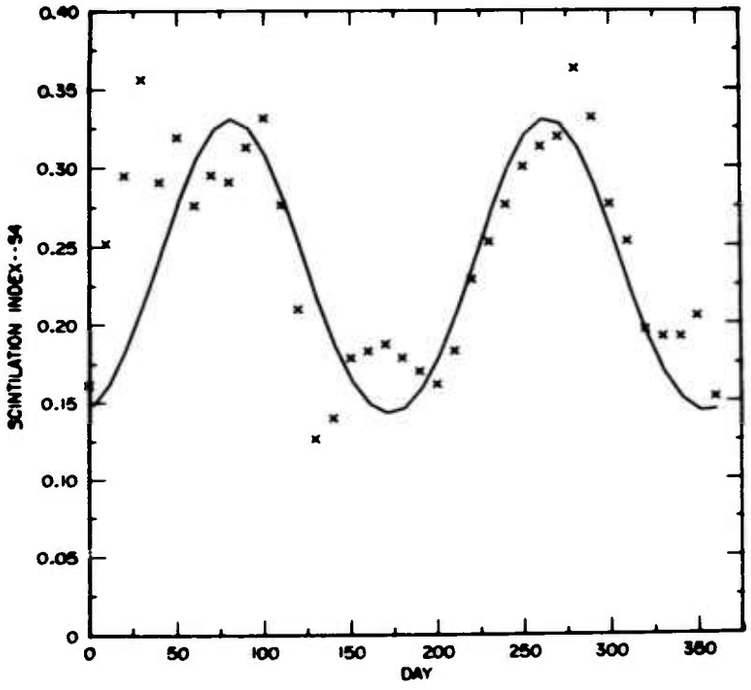

FIGURE 6 COMPARISON OF MODEL CALCULATION (solid curve) WITH THE SEASONAL VARIATION OF 136-MHz INTENSITY-SCINTILLATION INDEX OBSERVED (Xs) BY KOSTER (1968) IN THE EQUATORIAL REGION

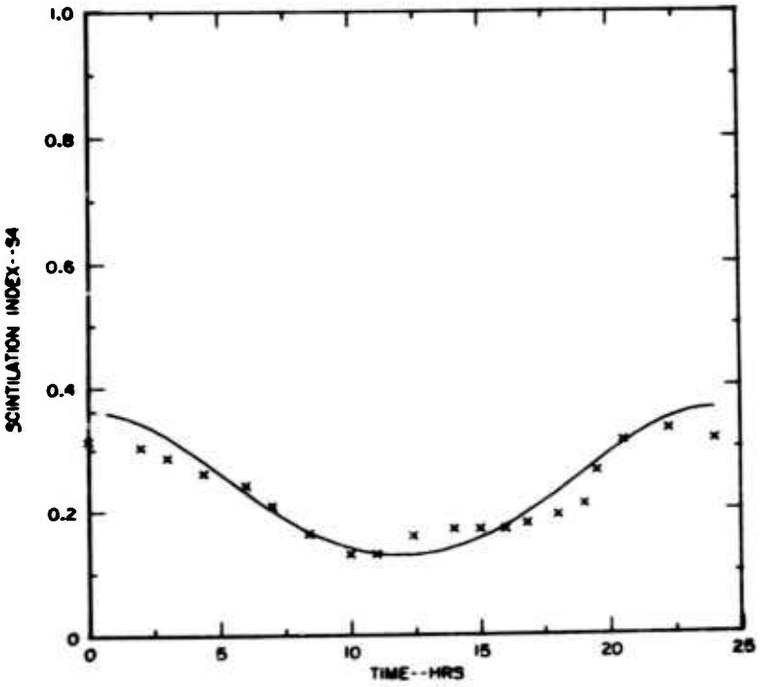

FIGURE 7 COMPARISON OF MODEL CALCULATION (solid curve) WITH DIURNAL VARIATION OF 40-MHz INTENSITY-SCINTILLATION INDEX OBSERVED (Xs) BY PREDDEY, MAWDSLEY, AND IRELAND (1969) IN THE MID-LATITUDE REGION

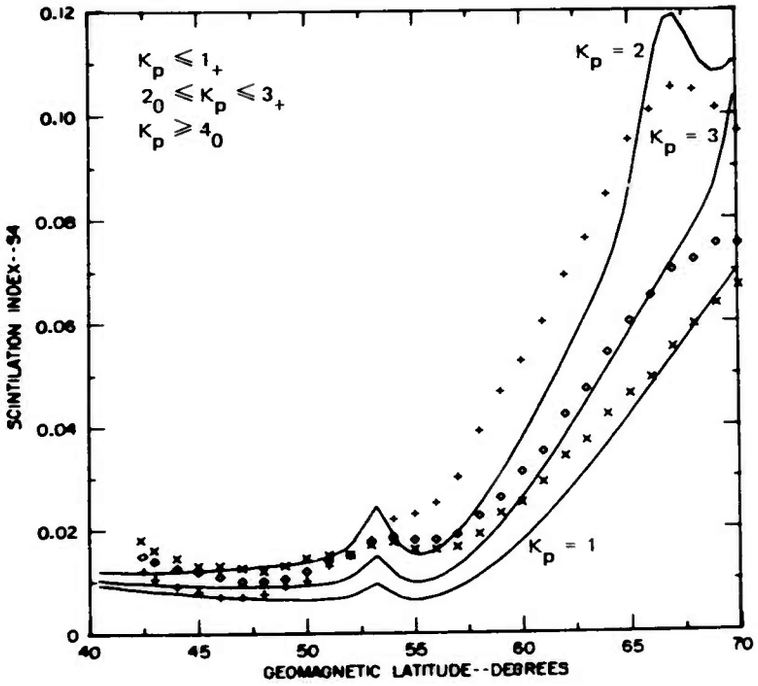

FIGURE 8 COMPARISON OF MODEL CALCULATIONS (solid curves) WITH THE LATITUDINAL VARIATION OF 400-MHz INTENSITY-SCINTILLATION INDEX, FOR THREE STATES OF GEOMAGNETIC DISTURBANCE, OBSERVED (symbols) BY EVANS (1973) NEAR THE SUBAURORAL SCINTILLATION BOUNDARY

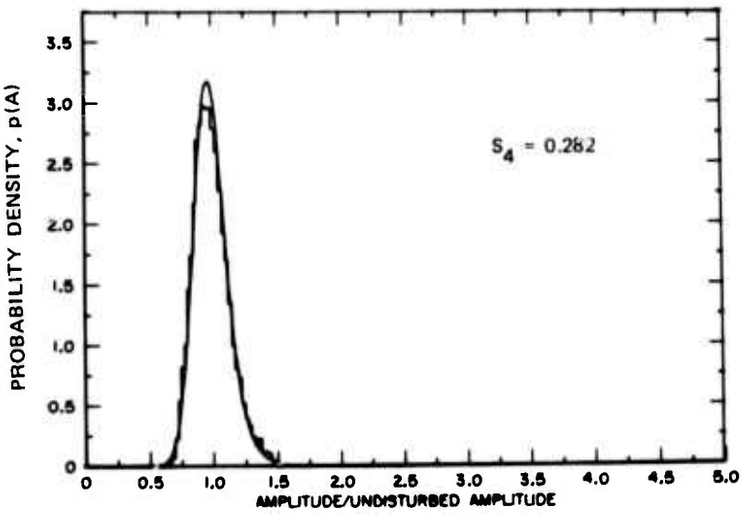

FIGURE 9 COMPARISON OF CALCULATED (smooth curve) PROBABILITY DENSITY FUNCTION FOR AMPLITUDE WITH OBSERVATIONS (histogram) OF ATS-5 TRANSMISSION AT 137 MHz, MADE BY AARONS (private communication, 1974) THROUGH THE MID-LATITUDE IONOSPHERE FROM NEAR BOSTON

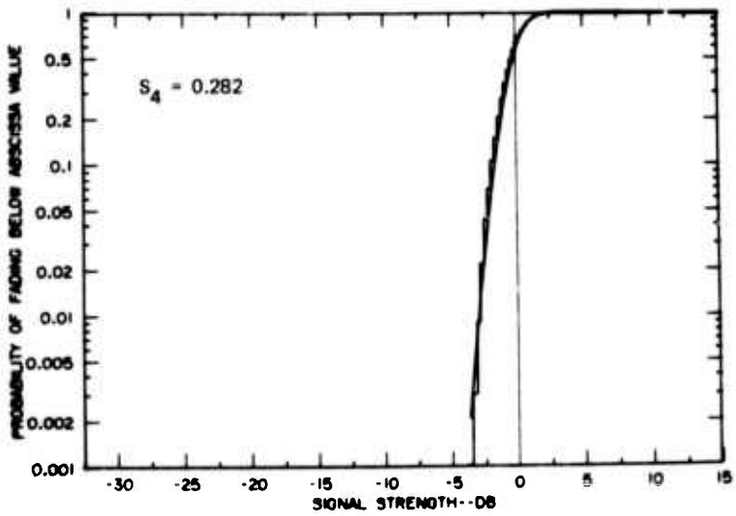

FIGURE 10 COMPARISON OF CALCULATED (smooth curve) CUMULATIVE PROBABILITY FUNCTION (cpf) FOR INTENSITY (or for amplitude) WITH OBSERVATIONS (histogram) FOR CASE IN FIGURE 9. (Calculations of cpf are intended for use in assessing fade-margin requirements.)

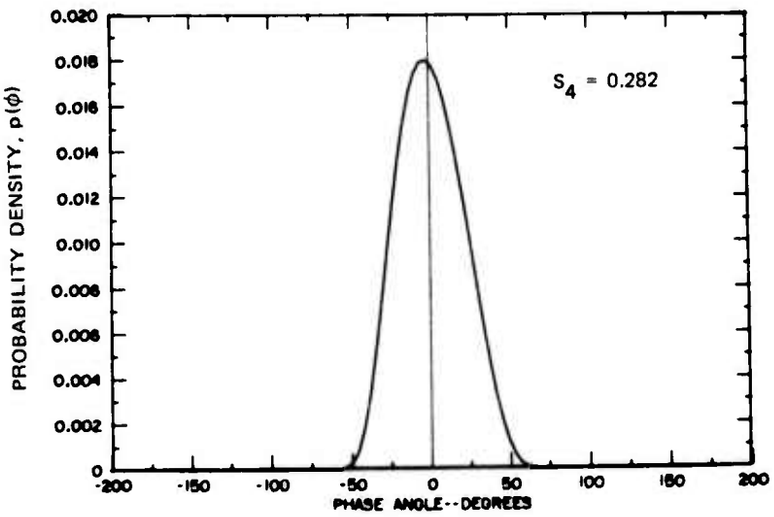

FIGURE 11 CALCULATED PROBABILITY DENSITY FUNCTION FOR PHASE FOR THE CASE IN FIGURES 9 AND 10. (No observed phase data exist for comparison.)

Table 1

ROUTINES IN PROGRAM RFMOD

Name	Function
BLOCK DATA	Initializes common parameters.
SUBROUTINE READIN, with ENTRY INC	Performs program inputting, and increments the changing parameter(s).
SUBROUTINE SCINT	Controls the basic scintillation calculation and provides quantities needed for SUBROUTINE SIGS.
SUBROUTINE SIGS	Performs the basic scintillation calculations.
FUNCTION RMSDN	Contains the worldwide model for strength of F-layer irregularities used in the scintillation calculation.
FUNCTION RFBPT	Evaluations the diffraction integral by an algebraic approximation.
SUBROUTINE FINDZ	Computes the reduced distance from scattering layer to receiver for use in evaluating Fresnel-zone radius.
SUBROUTINE MGFLD	Contains an earth-centered, axially tipped, dipole model of the geomagnetic field and calculates the geomagnetic coordinates of, and the field components at, a specified point.
SUBROUTINE AZNSIDE	Given the latitude and longitude of two points, A and B, computes the azimuth of B as seen from A and the great-circle arc AB.
SUBROUTINE COORD	Calculates coordinates of a desired point on a specified great-circle arc.
FUNCTION ERF	Computes the Error Function.
SUBROUTINE CPRMS	Controls calculation of rms phase.
FUNCTION PHAS, with ENTRY PRT	Evaluates the Hatfield phase distribution of a scintillating signal.
FUNCTION F1, with ENTRY F2	Provides integrand functions for evaluating moments of phase distribution.
SUBROUTINE SIMPA	Adaptively performs numerical integration using Simpson's rule.
SUBROUTINE IMPRIME	Performs program outputting.

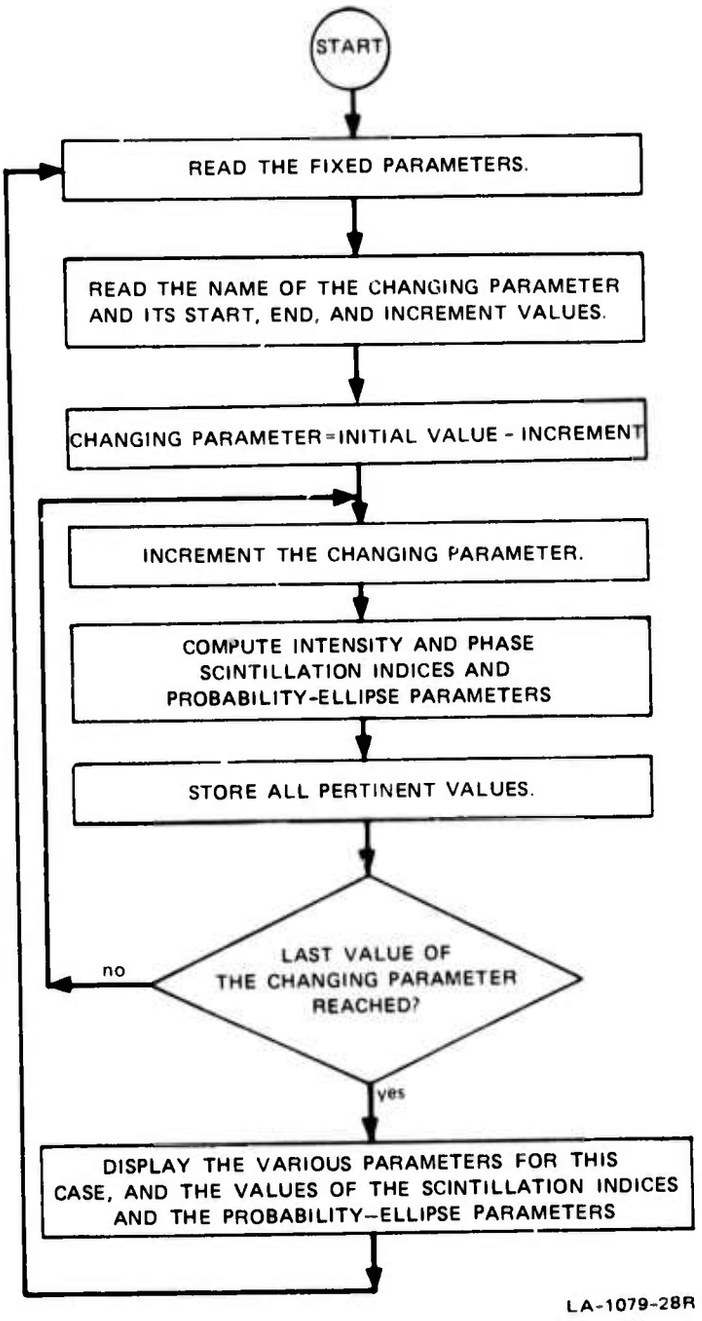

FIGURE 12 SIMPLIFIED FLOW CHART OF PROGRAM RFMOD

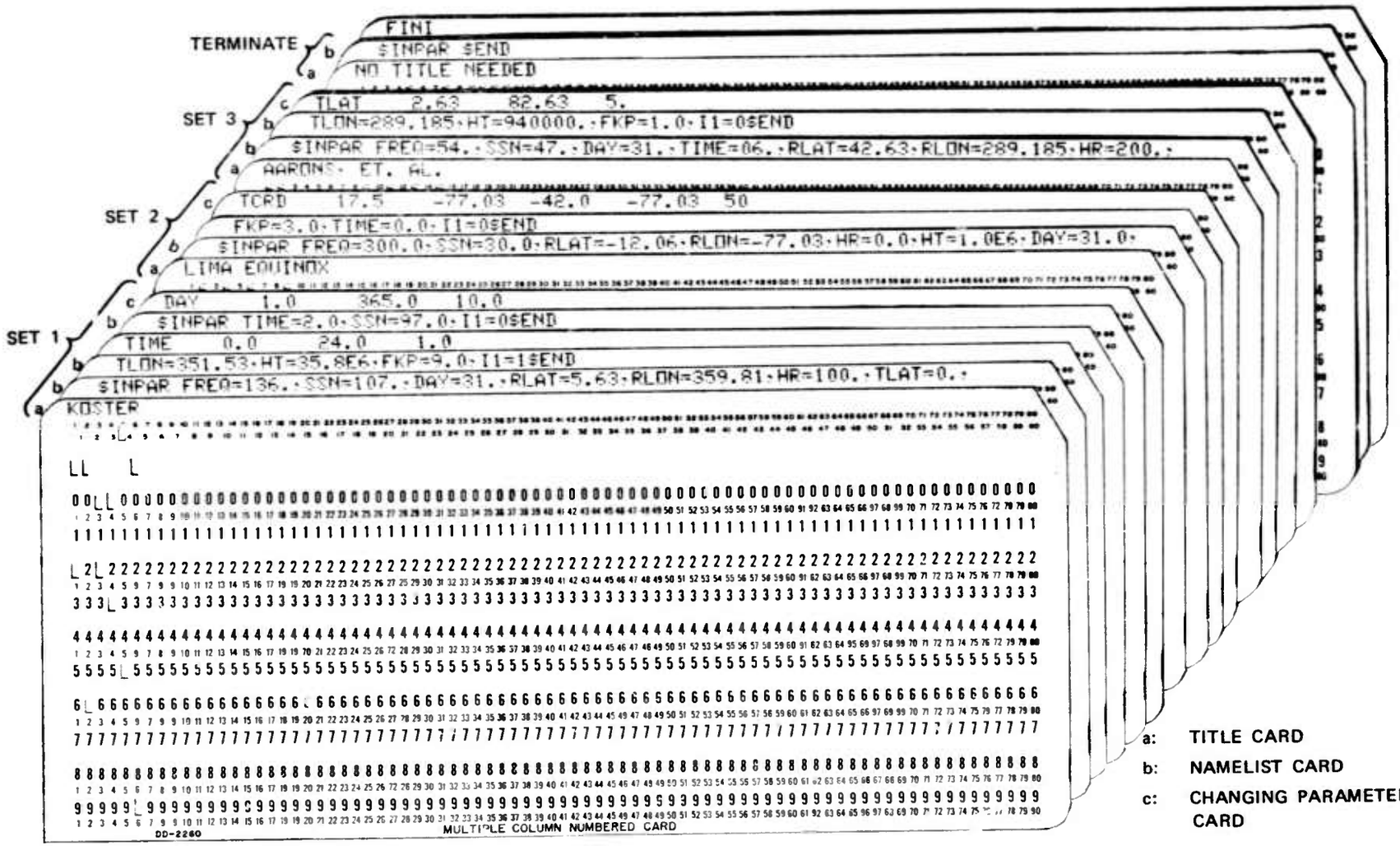

FIGURE 13 SAMPLE INPUT CARDS FOR PROGRAM RFMOD

Table 2

DATA-CARD VARIABLES

K	Variable Name	Unit	Definition
1	FREQ	Megahertz	Frequency
2	SSN	None (floating point)	Sunspot number
3	DAY	None (floating point)	Day of year
4	TIME	Decimal hours	Meridian time at ionospheric penetration point
5	RLAT	Decimal degrees	Receiver latitude
6	RLON	Decimal degrees	Receiver longitude
7	HR	Meters	Receiver altitude
8	TLAT	Decimal degrees	Transmitter latitude
9	TLON	Decimal degrees	Transmitter longitude
10	HT	Meters	Transmitter altitude
11	FKP	Decimal value 0.0 through 9.0	Planetary magnetic index, Kp
--	I1	None (value 1 or 0)	Data flag (see text)
12	RCRD	Decimal degrees	Receiver coordinates
13	TCRD	Decimal degrees	Transmitter coordinates

common VARPAR to identify the parameters. The user may list the fixed parameters in any order on the namelist cards.

A parameter input on a namelist card will keep the specified value until changed by means of a new namelist card or until input on a changing-parameter(s) card. The first column of each namelist card must be blank, and the first characters on the first namelist card must be &INPAR. The last namelist card in a sequence must terminate with the characters &END.

The changing-parameter(s) card is employed by the user to select the independent variable(s) for a given calculation case. He may choose either of two program modes. In Mode 1, he chooses any one of the parameters listed in Table 2 for which K is between 1 and 11, inclusive, and inputs its name on the changing-parameter card. In this mode, the first-order signal-statistical parameters, including S_4 and Φ_{rms}, are calculated as functions of the single changing parameter. In Figure 13, the cards identified as Set 1 are for two sequential cases run in Mode 1, under a common title.

Mode 2 permits the user to increment the position of either the receiver or the transmitter along an arc of a great circle. In this mode, both the latitude and longitude of the receiver or of the transmitter become changing parameters, and the signal-statistical parameters are calculated for equidistant points along the arc. Mode 2 is selected by naming RCRD or TCRD on the changing-parameters card (see Table 2). In Figure 13, the cards identified as Set 2 are for a run in this mode.

The required contents of the changing-parameter(s) card are listed in Table 3. Note that in Mode 1, if the final value of a changing parameter is smaller than the initial value, the increment value must be specified as negative. Absence of the required negative sign in this situation will cause the run to terminate, and an error message will be printed.

After reading a set of cards, the program will keep the same title and read only namelist and changing-parameter(s) cards, so long as I1 = 1. After encountering I1 = 0, it will read a new title card. The program will terminate if the name on the changing-parameter(s) card does not correspond to one of those numbered 1 through 13 in Table 2. Thus, to terminate a run, the user may prepare a changing-parameter card containing an unfamiliar word, such as the FINI appearing in Figure 13.

Table 3

CONTENTS OF CHANGING-PARAMETER(S) CARD

Columns	Mode-1 Content	Mode-2 Content	Symbol in Program
1 through 4	Name	Name	Name
9 through 16	Initial value	Initial latitude	A1
17 through 24	Final value	Initial longitude	A2
25 through 32	Increment value	Final latitude	A3
33 through 40	--	Final longitude	A4
41 through 42	--	Number of increments	NA5

For model development and testing, we employed a plotting routine in conjunction with RFMOD to produce graphs such as those in Figures 5 through 8. The available version of RFMOD provides an array that the user may employ with his own computer peripherals. In the absence of user modification, the array will be output in tabular form along with identifying information, as shown for a test case in Figure 14. In the case shown, the changing parameter was the latitude of the transmitter, which was taken to be in a polar-orbiting satellite passing over a receiving station near Boston (namely, the Sagamore Hill site of the AFCRL group headed by Aarons). The changing parameter is followed in each row by the azimuth and elevation of the satellite, the three probability-ellipse parameters, and then by the calculated scintillation indices. The input cards for this run are identified as Set 3 in Figure 13.

It is envisioned that a user will inspect the values of S4 and/or PRMS predicted for his communication link by RFMOD and then decide if he wants more detailed signal-statistical information for a particular situation. In the example of Figure 14, for instance, he might decide

F-LAYER PRODUCED VHF-UHF SCINTILLATION

CALCULATED FROM A MODEL DEVELOPED BY STANFORD RESEARCH INSTITUTE,
MENLO PARK, CALIFORNIA.

***AARONS, FT. AL.

INPUT CONDITIONS USED FOR THIS CALCULATION WERE :

FREQUENCY= 54.000 MHZ SUNSPOT NO.= 47. DAY 31. OUT OF 365 KP INDEX = 1.00 TIME= 6.00

RECEIVER COORDINATES LAT= 42.63 DEG LONG= 289.18 DEG ALT= .200 KM
TRANSMITTER COORDINATES LONG= 289.18 DEG ALT= 940.000 KM

(FOR THIS RUN, THE CHANGING PARAMETER WAS: TRANSMITTER LATITUDE)

TLAT	AZ	EL	RZRO	RMAGR	DELTA	S4	PRMS
17.63	180.00	4.71	.088	.896	4.662	.178	16.172
22.63	180.00	11.28	.071	.908	4.140	.148	14.614
27.63	180.00	20.05	.071	.923	3.474	.139	14.638
32.63	180.00	33.13	.089	.937	2.822	.154	16.334
37.63	180.00	55.06	.194	.944	2.512	.293	23.796
42.63	180.00	90.00	.155	.954	2.073	.235	21.432
47.63	0.00	55.06	.124	.951	2.220	.194	19.201
52.63	0.00	33.13	.205	.939	2.742	.311	24.448
57.63	0.00	20.05	.371	.924	3.419	.538	32.835
62.63	0.00	11.28	.605	.909	4.090	.845	43.736
67.63	0.00	4.71	.821*	.898	4.607	1.117	57.215

* SINGLE-SCATTER APPROX. WARNING

FIGURE 14 EXAMPLE OF OUTPUT FROM AVAILABL VERSION OF PROGRAM RFMOD

that he wants the full first-order distributions of intensity and phase for the case in which S4 on his channel is .538 and PRMS is 32.835 degrees. To obtain the distributions he would employ DIST, inputting RZRO = .371, BMAGR = .924, and DELTA = 3.419 degrees, on a single card in F10.3 format. The DIST code consists of the routines listed in Table 4.

Table 4

ROUTINES IN PROGRAM DIST

Name	Function
SUBROUTINE PDFI	Controls calculation and output of probability density function for amplitude, by means of one-dimensional integration over two-dimensional Gaussian probability density function.
SUBROUTINE PARRAY	Initializes amplitude array for SUBROUTINE PDFI.
SUBROUTINE GAUP	Controls calculation of Gaussian probability density function.
FUNCTION PR	Computes two-dimensional Gaussian probability density function.
FUNCTION XINTGR	Performs integration by Simpson's rule.
SUBROUTINE PDFP	Controls computation and output of probability density function for phase, calling SUBROUTINE PHA3.
SUBROUTINE PHAS	Evaluates Hatfield phase distribution.
FUNCTION ERF	Computes the Error Function.
SUBROUTINE CPFI	Calculates and outputs the cumulative probability density function for amplitude or intensity (expressed in dB) by performing Simpson's rule integration over probability density function for amplitude.

Again, for modeling we employ a plotting routine in conjunction with DIST to produce graphs such as those in 9, 10, and 11. The available version of DIST simply outputs the array from which such graphs are made, in the line-printer formats shown in Figures 15, 16, and 17. As with RFMOD, a user may wish to employ DIST in conjunction with his own plotting routine or in some other output form. Alternatively, he may wish to reformat the array listing, perhaps outputting fewer values and possibly presenting CPF in terms of percent or decimal link reliability (the one's complement of CPF) rather than directly as in Figure 16.

V CONCLUSION

It has been our attempt to develop a channel model that may be used conveniently for calculating first-order signal statistics, expressed in a format relevant to systems application. The resulting codes, RFMOD and DIST, represent the first-year output of a broader effort to definitively model the transionospheric communication channel. These codes are to be augmented by routines to permit calculation of second-order statistics, such as fluctuation spectra of amplitude and phase, as well as signal correlation at spaced receivers and across bands of frequency. Moreover, the existing version of RFMOD is likely to evolve over the next year in two important ways.

First, it is intended to modify SUBROUTINE SIGS in RFMOD to fully account for multiple scatter. Theoretical work now underway is hinting at a possible form for the modification. The single-scatter theory described in Section II of this report describes the simultaneous rotation (increasing δ) and circularization (decreasing $|B_o|/R_o$) of the first-order probability ellipse for the received signal's complex amplitude (illustrated in Figure 1), as the wave propagates away from the scattered medium. In the single-scatter limit, the ellipse emerges from

PROBABILITY DENSITY, P(A), VS. AMPLITUDE/UNDISTURBED AMPLITUDE
FOR RZNO= .37 BMAGR= .92 DELTA= 3.42

A	P(A)	A	P(A)	A	P(A)	A	P(A)	A	P(A)	A	P(A)	A	P(A)	A	P(A)
0.0000	0.0000	.0125	.0000	.0250	.0000	.0375	.0000	.0500	.0000	.0625	.0000	.0750	.0000	.0875	.0000
.1000	.0000	.1125	.0000	.1250	.0000	.1375	.0000	.1500	.0000	.1625	.0000	.1750	.0000	.1875	.0000
.2000	.0000	.2125	.0000	.2250	.0000	.2375	.0000	.2500	.0000	.2625	.0000	.2750	.0000	.2875	.0001
.3000	.0001	.3125	.0002	.3250	.0002	.3375	.0004	.3500	.0006	.3625	.0009	.3750	.0013	.3875	.0019
.4000	.0028	.4125	.0041	.4250	.0058	.4375	.0083	.4500	.0116	.4625	.0160	.4750	.0220	.4875	.0298
.5000	.0400	.5125	.0530	.5250	.0695	.5375	.0902	.5500	.1158	.5625	.1471	.5750	.1848	.5875	.2298
.6000	.2827	.6125	.3442	.6250	.4147	.6375	.4945	.6500	.5835	.6625	.6816	.6750	.7881	.6875	.9021
.7000	1.0223	.7125	1.1471	.7250	1.2747	.7375	1.4029	.7500	1.5293	.7625	1.6515	.7750	1.7670	.7875	1.8736
.8000	1.9691	.8125	2.0516	.8250	2.1195	.8375	2.1717	.8500	2.2076	.8625	2.2269	.8750	2.2300	.8875	2.2174
.9000	2.1901	.9125	2.1497	.9250	2.0976	.9375	2.0357	.9500	1.9657	.9625	1.8896	.9750	1.8090	.9875	1.7257
1.0000	1.6413	1.0125	1.5569	1.0250	1.4737	1.0375	1.3967	1.0500	1.3145	1.0625	1.2396	1.0750	1.1683	1.0875	1.1010
1.1000	1.0375	1.1125	.9779	1.1250	.9221	1.1375	.8698	1.1500	.8210	1.1625	.7754	1.1750	.7327	1.1875	.6928
1.2000	.6553	1.2125	.6202	1.2250	.5872	1.2375	.5561	1.2500	.5269	1.2625	.4993	1.2750	.4732	1.2875	.4485
1.3000	.4252	1.3125	.4030	1.3250	.3821	1.3375	.3621	1.3500	.3432	1.3625	.3253	1.3750	.3082	1.3875	.2920
1.4000	.2766	1.4125	.2620	1.4250	.2481	1.4375	.2348	1.4500	.2222	1.4625	.2103	1.4750	.1989	1.4875	.1881
1.5000	.1778	1.5125	.1681	1.5250	.1588	1.5375	.1500	1.5500	.1417	1.5625	.1337	1.5750	.1262	1.5875	.1190
1.6000	.1123	1.6125	.1058	1.6250	.0997	1.6375	.0940	1.6500	.0885	1.6625	.0833	1.6750	.0784	1.6875	.0738
1.7000	.0694	1.7125	.0652	1.7250	.0613	1.7375	.0576	1.7500	.0540	1.7625	.0507	1.7750	.0476	1.7875	.0446
1.8000	.0419	1.8125	.0392	1.8250	.0368	1.8375	.0344	1.8500	.0322	1.8625	.0302	1.8750	.0282	1.8875	.0264
1.9000	.0247	1.9125	.0230	1.9250	.0215	1.9375	.0201	1.9500	.0187	1.9625	.0175	1.9750	.0163	1.9875	.0152
2.0000	.0142	2.0125	.0132	2.0250	.0123	2.0375	.0114	2.0500	.0106	2.0625	.0099	2.0750	.0092	2.0875	.0085
2.1000	.0079	2.1125	.0073	2.1250	.0068	2.1375	.0063	2.1500	.0059	2.1625	.0054	2.1750	.0050	2.1875	.0047
2.2000	.0043	2.2125	.0040	2.2250	.0037	2.2375	.0034	2.2500	.0032	2.2625	.0029	2.2750	.0027	2.2875	.0025
2.3000	.0023	2.3125	.0021	2.3250	.0019	2.3375	.0018	2.3500	.0017	2.3625	.0015	2.3750	.0014	2.3875	.0013
2.4000	.0012	2.4125	.0011	2.4250	.0010	2.4375	.0009	2.4500	.0008	2.4625	.0008	2.4750	.0007	2.4875	.0006
2.5000	.0006	2.5125	.0005	2.5250	.0005	2.5375	.0005	2.5500	.0004	2.5625	.0004	2.5750	.0003	2.5875	.0003
2.6000	.0003	2.6125	.0003	2.6250	.0002	2.6375	.0002	2.6500	.0002	2.6625	.0002	2.6750	.0002	2.6875	.0002
2.7000	.0001	2.7125	.0001	2.7250	.0001	2.7375	.0001	2.7500	.0001	2.7625	.0001	2.7750	.0001	2.7875	.0001
2.8000	.0001	2.8125	.0001	2.8250	.0001	2.8375	.0000	2.8500	.0000	2.8625	.0000	2.8750	.0000	2.8875	.0000
2.9000	.0000	2.9125	.0000	2.9250	.0000	2.9375	.0000	2.9500	.0000	2.9625	.0000	2.9750	.0000	2.9875	.0000
3.0000	.0000	3.0125	.0000	3.0250	.0000	3.0375	.0000	3.0500	.0000	3.0625	.0000	3.0750	.0000	3.0875	.0000
3.1000	.0000	3.1125	.0000	3.1250	.0000	3.1375	.0000	3.1500	.0000	3.1625	.0000	3.1750	.0000	3.1875	.0000
3.2000	.0000	3.2125	.0000	3.2250	.0000	3.2375	.0000	3.2500	.0000	3.2625	.0000	3.2750	.0000	3.2875	.0000
3.3000	.0000	3.3125	.0000	3.3250	.0000	3.3375	.0000	3.3500	.0000	3.3625	.0000	3.3750	.0000	3.3875	.0000
3.4000	.0000	3.4125	.0000	3.4250	.0000	3.4375	.0000	3.4500	.0000	3.4625	.0000	3.4750	.0000	3.4875	.0000
3.5000	.0000	3.5125	.0000	3.5250	.0000	3.5375	.0000	3.5500	.0000	3.5625	.0000	3.5750	.0000	3.5875	.0000
3.6000	.0000	3.6125	.0000	3.6250	.0000	3.6375	.0000	3.6500	.0000	3.6625	.0000	3.6750	.0000	3.6875	.0000
3.7000	.0000	3.7125	.0000	3.7250	.0000	3.7375	.0000	3.7500	.0000	3.7625	.0000	3.7750	.0000	3.7875	.0000
3.8000	.0000	3.8125	.0000	3.8250	.0000	3.8375	.0000	3.8500	.0000	3.8625	.0000	3.8750	.0000	3.8875	.0000
3.9000	.0000	3.9125	.0000	3.9250	.0000	3.9375	.0000	3.9500	.0000	3.9625	.0000	3.9750	.0000	3.9875	.0000
4.0000	.0000	4.0125	.0000	4.0250	.0000	4.0375	.0000	4.0500	.0000	4.0625	.0000	4.0750	.0000	4.0875	.0000
4.1000	.0000	4.1125	.0000	4.1250	.0000	4.1375	.0000	4.1500	.0000	4.1625	.0000	4.1750	.0000	4.1875	.0000
4.2000	.0000	4.2125	.0000	4.2250	.0000	4.2375	.0000	4.2500	.0000	4.2625	.0000	4.2750	.0000	4.2875	.0000
4.3000	.0000	4.3125	.0000	4.3250	.0000	4.3375	.0000	4.3500	.0000	4.3625	.0000	4.3750	.0000	4.3875	.0000
4.4000	.0000	4.4125	.0000	4.4250	.0000	4.4375	.0000	4.4500	.0000	4.4625	.0000	4.4750	.0000	4.4875	.0000
4.5000	.0000	4.5125	.0000	4.5250	.0000	4.5375	.0000	4.5500	.0000	4.5625	.0000	4.5750	.0000	4.5875	.0000
4.6000	.0000	4.6125	.0000	4.6250	.0000	4.6375	.0000	4.6500	.0000	4.6625	.0000	4.6750	.0000	4.6875	.0000
4.7000	.0000	4.7125	.0000	4.7250	.0000	4.7375	.0000	4.7500	.0000	4.7625	.0000	4.7750	.0000	4.7875	.0000
4.8000	.0000	4.8125	.0000	4.8250	.0000	4.8375	.0000	4.8500	.0000	4.8625	.0000	4.8750	.0000	4.8875	.0000
4.9000	.0000	4.9125	.0000	4.9250	.0000	4.9375	.0000	4.9500	.0000	4.9625	.0000	4.9750	.0000	4.9875	.0000
5.0000	.0000														

FIGURE 15 EXAMPLE OF AMPLITUDE pdf OUTPUT FROM AVAILABLE VERSION OF PROGRAM DIST

CUMULATIVE PROBABILITY, CPF, VS. SIGNAL STRENGTH IN DB RELATIVE TO UNDISTURBED LEVEL
FOR RZRO= .37 RMAGR= .92 DELTA= 3.42

DB	CPF	DB	CPF	DB	CPF	DB	CPF	DB	CPF	DB	CPF	DB	CPF	DB	CPF
-32.04	.0000	-26.02	.0000	-22.50	.0000	-20.00	.0000	-18.06	.0000	-16.48	.0000	-15.14	.0000	-13.98	.0000
-12.96	.0000	-12.04	.0000	-11.21	.0000	-10.46	.0000	-9.76	.0000	-9.12	.0000	-8.52	.0000	-7.96	.0001
-7.43	.0002	-6.94	.0004	-6.47	.0008	-6.02	.0016	-5.60	.0029	-5.19	.0052	-4.81	.0089	-4.44	.0147
-4.08	.0239	-3.74	.0357	-3.41	.0526	-3.10	.0754	-2.79	.1040	-2.50	.1391	-2.21	.1804	-1.94	.2272
-1.67	.2784	-1.41	.3326	-1.16	.3882	-.92	.4436	-.68	.4973	-.45	.5481	-.22	.5954	-.00	.6385
.21	.6774	.42	.7123	.63	.7433	.83	.7708	1.02	.7953	1.21	.8170	1.40	.8364	1.58	.8538
1.76	.8693	1.94	.8832	2.11	.8957	2.28	.9069	2.44	.9170	2.61	.9260	2.77	.9342	2.92	.9415
3.08	.9480	3.23	.9539	3.38	.9592	3.52	.9639	3.67	.9681	3.81	.9718	3.95	.9752	4.08	.9781
4.22	.9808	4.35	.9831	4.48	.9852	4.61	.9871	4.74	.9887	4.86	.9901	4.98	.9914	5.11	.9925
5.23	.9935	5.34	.9944	5.46	.9951	5.58	.9958	5.69	.9964	5.80	.9969	5.91	.9973	6.02	.9977
6.13	.9980	6.24	.9983	6.34	.9985	6.44	.9988	6.55	.9989	6.65	.9991	6.75	.9992	6.85	.9993
6.95	.9994	7.04	.9995	7.14	.9996	7.23	.9997	7.33	.9997	7.42	.9998	7.51	.9998	7.60	.9998
7.69	.9999	7.78	.9999	7.87	.9999	7.96	.9999	8.05	.9999	8.13	.9999	8.22	1.0000	8.30	1.0000
8.38	1.0000	8.46	1.0000	8.55	1.0000	8.63	1.0000	8.71	1.0000	8.79	1.0000	8.87	1.0000	8.94	1.0000
9.02	1.0000	9.10	1.0000	9.17	1.0000	9.25	1.0000	9.32	1.0000	9.40	1.0000	9.47	1.0000	9.54	1.0000
9.61	1.0000	9.69	1.0000	9.76	1.0000	9.83	1.0000	9.90	1.0000	9.97	1.0000	10.03	1.0000	10.10	1.0000
10.17	1.0000	10.24	1.0000	10.30	1.0000	10.37	1.0000	10.44	1.0000	10.50	1.0000	10.57	1.0000	10.63	1.0000
10.69	1.0000	10.76	1.0000	10.82	1.0000	10.88	1.0000	10.94	1.0000	11.00	1.0000	11.07	1.0000	11.13	1.0000
11.19	1.0000	11.25	1.0000	11.31	1.0000	11.36	1.0000	11.42	1.0000	11.48	1.0000	11.54	1.0000	11.60	1.0000
11.65	1.0000	11.71	1.0000	11.77	1.0000	11.82	1.0000	11.88	1.0000	11.93	1.0000	11.99	1.0000	12.04	1.0000
12.10	1.0000	12.15	1.0000	12.20	1.0000	12.26	1.0000	12.31	1.0000	12.36	1.0000	12.41	1.0000	12.46	1.0000
12.52	1.0000	12.57	1.0000	12.62	1.0000	12.67	1.0000	12.72	1.0000	12.77	1.0000	12.82	1.0000	12.87	1.0000
12.92	1.0000	12.97	1.0000	13.02	1.0000	13.06	1.0000	13.11	1.0000	13.16	1.0000	13.21	1.0000	13.26	1.0000
13.30	1.0000	13.35	1.0000	13.40	1.0000	13.44	1.0000	13.49	1.0000	13.53	1.0000	13.58	1.0000	13.62	1.0000
13.67	1.0000	13.71	1.0000	13.76	1.0000	13.80	1.0000	13.85	1.0000	13.89	1.0000	13.94	1.0000	13.98	1.0000

FIGURE 16 EXAMPLE OF cdf OUTPUT FROM AVAILABLE VERSION OF PROGRAM DIST

PROBABILITY DENSITY, P(PHI), VS. PHASE ANGLE IN DEGREES
FOR RZRO= .37 RMAGR= .92 DELTA= 3.42

PHI	P(PHI)	PHI	P(PHI)	PHI	P(PHI)	PHI	P(PHI)	PHI	P(PHI)	PHI	P(PHI)	PHI	P(PHI)	PHI	P(PHI)
-180.00	.0000	-176.36	.0000	-172.73	.0000	-169.09	.0000	-165.45	.0000	-161.82	.0000	-158.18	.0000	-154.55	.0000
-150.91	.0000	-147.27	.0000	-143.64	.0000	-140.00	.0000	-136.36	.0000	-132.73	.0000	-129.09	.0000	-125.45	.0000
-121.82	.0000	-118.18	.0000	-114.55	.0000	-110.91	.0000	-107.27	.0000	-103.64	.0000	-100.00	.0000	-96.36	.0000
-92.73	.0000	-89.09	.0000	-85.45	.0000	-81.82	.0000	-78.18	.0000	-74.55	.0000	-70.91	.0001	-67.27	.0003
-63.64	.0010	-60.00	.0021	-56.36	.0036	-52.73	.0050	-49.09	.0063	-45.45	.0074	-41.82	.0082	-38.18	.0088
-34.55	.0092	-30.91	.0094	-27.27	.0096	-23.64	.0096	-20.00	.0096	-16.36	.0096	-12.73	.0095	-9.09	.0094
-5.45	.0094	-1.82	.0093	1.82	.0092	5.45	.0092	9.09	.0091	12.73	.0091	16.36	.0090	20.00	.0089
23.64	.0089	27.27	.0087	30.91	.0086	34.55	.0084	38.18	.0081	41.82	.0078	45.45	.0073	49.09	.0066
52.73	.0058	56.36	.0048	60.00	.0036	63.64	.0024	67.27	.0014	70.91	.0006	74.55	.0002	78.18	.0000
81.82	.0000	85.45	.0000	89.09	.0000	92.73	.0000	96.36	.0000	100.00	.0000	103.64	.0000	107.27	.0000
110.91	.0000	114.55	.0000	118.18	.0000	121.82	.0000	125.45	.0000	129.09	.0000	132.73	.0000	136.36	.0000
140.00	.0000	143.64	.0000	147.27	.0000	150.91	.0000	154.55	.0000	158.18	.0000	161.82	.0000	165.45	.0000
169.09	.0000	172.73	.0000	176.36	.0000	180.00	.0000								

FIGURE 17 EXAMPLE OF PHASE pdf OUTPUT FROM AVAILABLE VERSION OF PROGRAM DIST

the scattering layer highly elongated ($|B_o|/R_o \approx 1$) and oriented nearly vertically ($\delta \approx 0$) on the complex plane.

Multiple-scatter calculations for the special case of normal incidence on the scattering layer show that some circularization ($|B_o|/R_o \approx e^{-R_o}$), but no rotation ($\delta \approx 0$), is produced by the rescatterings. This is an intuitively understandable result and, if corroborated by similar calculations for off-normal incidence, is expected to lead to a multiple-scatter correction for $|B_o|/R_o$ analogous to Eq. (28) for R_o. It will presumably also lead to a modification of Eq. (24) for relating the ellipse orientation to its elongation at the receiver. The result is certain to be a reduction in the third term of Eq. (5) for intensity-scintillation index as the fraction of flux scattered (R_o) increases. It will presumably limit values of S_4 to something near unity and improve agreement between calculated and observed values for moderate to strong scintillation.

The other important area in which RFMOD is expected to evolve is that of scintillation morphology, which will entail updating of FUNCTION RMSDN. As more definitive scintillation data become available, the model of electron-density irregularity strength contained in RMSDN presumably will be improved by a process that may be viewed as calibration [i.e., the main changes should be adjustment of the coefficients in Eqs. (42) through (45)]. This will be particularly so in regions where the model is currently calibrated in terms of ad hoc indices such as SI instead of in terms of S_4. One such region is the important one centered on the geomagnetic equator. Useful equatorial data are expected from observations of the NOAA ionospheric beacon on board NASA's ATS-6, particularly measurements of S_4 at 140 and 360 MHz. During periods of weak to moderate scintillation, estimates should also be obtained of ϕ_{rms} at 140 MHz. The ATS-6 observations also will provide histograms

of amplitude (under all conditions)) and of phase (under conditions of weak to moderate scintillation) for testing the predictions made by the DIST code.

Pending the improvements described above, we offer RFMOD and DIST as the best way to estimate the first-order signal statistics to be expected at the output of a user's transionospheric communication link, short of performing a series of observations over that particular link. It must be remembered that the estimated values are those expected for average ionospheric conditions in the observing situation (frequency, transmitter and receiver location, time of day, K_p, etc.) specified by the user. There is presumably some statistical distribution of each parameter estimated about its calculated value, and the present model does not account for such statistical variation. Possibly of equal importance, the model has yet to be subjected to testing against observations above 400 MHz (e.g., in the SHF band).

REFERENCES

Aarons, J., J. P. Mullen, and S. Basu, "Geomagnetic Control of Satellite Scintillations," J. Geophys. Res., Vol. 68, No. 10, pp. 3159-3168 (1963).

Aarons, J., J. P. Mullen, and H. E. Whitney, "The Scintillation Boundary," J. Geophys. Res., Vol. 74, No. 3, pp. 884-889 (1969).

Beckman, P., and A. Spizzichino, The Scattering of Electromagnetic Waves from Rough Surfaces, pp. 119-136 (Pergamon Press, New York, New York, 1963).

Bramley, E. N., "Some Aspects of the Rapid Directional Fluctuations of Short Radio Waves Reflected at the Ionosphere," Proc. IEEE, Vol. 102, pp. 533-540 (1955).

Briggs, B. H., and I. A. Parkin, "On the Variation of Radio Star and Satellite Scintillations with Zenith Angle," J. Atmos. Terr. Phys., Vol. 25, pp. 339-365 (1963).

Budden, K. G., "The Amplitude Fluctuations of the Radio Wave Scattered from a Thick Ionospheric Layer with Weak Irregularities," J. Atmos. Terr. Phys., Vol. 27, pp. 155-172 (1965).

de la Beaujardiere, O., and D. McNiel, "A Fortran Program for Calculating F-Layer-Produced Scintillation," Final Report, SRI Project 1079, Contract NAS5-21551, Stanford Research Institute, Menlo Park, California (December 1971).

Dyson, P. L., J. P. McClure, and W. B. Hanson, "In Situ Measurements of the Spectral Characteristics of F Region Ionospheric Irregularities," J. Geophys. Res., Vol. 79, No. 10, pp. 1497-1502 (1 April 1974).

Evans, J. V., Ed., "Millstone Hill Radar Propagation Study: Scientific Results--Part II," Technical Report 509, Lincoln Laboratory, Massachusetts Institute of Technology, Lexington, Massachusetts (12 November 1973).

Fejer, J. A., "The Diffraction of Waves in Passing Through an Irregular Refracting Medium," Proc. Roy. Soc. A., Vol. 220 (1953).

Fremouw, E. J., Ed., "An Experiment to Measure Trans-Atmospheric Wideband Radio Propagation Parameters," Final Report--Phase I, Contract DASA01-68-C-0104, DASA Report DASA-2362-1, SRI Project 7161, Stanford Research Institute, Menlo Park, California (1969).

Fremouw, E. J., "Measurement of Phase Variance and Autocorrelation During Radio-Star Visibility Fades," J. Geophys. Res., Vol. 73, No. 11, pp. 3557-3564 (1968).

Fremouw, E. J., and C. L. Rino, "An Empirical Model for Average F-Layer Scintillation at VHF/UHF," Radio Science, Vol. 8, No. 3, pp. 213-222 (March 1973).

Hatfield, V. E., "Non-Rician Statistics and Their Implications for Modeling Effects of Scintillation on Communication Channels," paper presented at NRL Symposium on Effects of the Ionosphere on Space Systems and Communication, Washington, D.C., 20-22 January 1975.

JSSG [Joint Satellite Studies Group], "On the Latitude Variation of Scintillations of Ionosphere Origin in Satellite Signals," Planet. Space Sci., Vol. 16, No. 6, pp. 775-781 (1968).

Koster, J. R., "Equatorial Studies of the VHF Signal Radiated by Intelstat II, F-3, 1, Ionospheric Scintillation," Progress Report 3, Contract F61052-67-C00026, University of Ghana-Legon, Accra, Ghana.

Nakagami, M., "The m-Distribution--A General Formula of Intensity Distribution of Rapid Fading," Stat. Methods in Radio Wave Prop., W. C. Hoffman, ed., pp. 3-36 (Pergamon Press, Oxford, 1960).

Pope, J. H., "High-Latitude Ionospheric Irregularity Model," Radio Science, Vol. 9, No. 7, pp. 576-682 (1974).

Rino, C. L., "Analysis of Scintillation Effects on Communication and Radar Systems," Bimonthly Progress Report 4, SRI Project 3399, Contract DNA001-74-C-0255, Stanford Research Institute, Menlo Park, California (15 January 1975).

Rino, C. L., and E. J. Fremouw, "Statistics for Ionospherically Diffracted VHF/UHF Signals," Radio Science, Vol. 8, No. 3, pp. 223-233 (March 1973a).

Rino, C. L., and E. J. Fremouw, "Ionospheric Scintillation Studies," Final Report, Contract NAS5-21891, SRI Project 2273, Stanford Research Institute, Menlo Park, California (November 1973b).

Rino, C. L., R. C. Livingston, and H. E. Whitney, "Some New Results on the Statistics of Radio-Wave Scintillation: A. Empirical Evidence for Gaussian Statistics," accepted for publication in J. Geophys. Res., 1975.

Rufenach, C. L., "Power-Law Wavenumber Spectrum Deduced from Ionospheric Scintillation Observations," J. Geophys. Res., Vol. 77, No. 25, pp. 4761-4772 (1 September 1972).

Sagalyn, R., M. Smiddy, and M. Ahmed, "High-Latitude Irregularities in the Top Side Ionosphere Based on ISIS I Thermal Ion Probe Data," J. Geophys. Res., Vol. 79, No. 28, pp. 4252-4261 (October 1974).

Whitney, H. E., "Notes on the Relationship of Scintillation Index to Probability Distributions and Their Uses for System Design," Environmental Research Papers No. 461, Report No. AFCRL-TR-74-0004, Ionospheric Physics Laboratory, Air Force Cambridge Research Laboratories, L. G. Hanscom Field, Bedford, Massachusetts (January 1974).

Whitney, H. E., and C. Malik, "A Proposed Index for Measuring Ionospheric Scintillation," Environmental Research Papers No. 284, Report No. AFCRL-68-0138, Ionospheric Physics Laboratory Air Force Cambridge Research Laboratories, L. G. Hanscom Field, Bedford, Massachusetts (March 1968).